



S. Mostafa Ghiaasiaan

Contents

1	Introduction	1698
2	Pool Boiling	1698
2.1	The Pool Boiling Regimes and Pool Boiling Curve	1698
2.2	Boiling Curve Hysteresis	1701
2.3	Parametric Effects	1707
2.4	Film Boiling	1709
2.5	The Effect of Thermal Radiation in Film Boiling	1723
2.6	Minimum Film Boiling Heat Flux and Temperature	1725
2.7	Transition Boiling	1732
3	Flow Boiling	1734
3.1	Forced-Flow Boiling Regimes	1735
3.2	Minimum Film Boiling Point and Transition Boiling	1738
3.3	Stable Film Boiling and Dispersed Flow Film Boiling	1740
4	Cross-References	1742
	References	1742

Abstract

Transition boiling, minimum film boiling (minimum heat flux), and film boiling are reviewed. The review will address pool and external flow boiling in Sect. 2. A discussion of internal flow boiling, with emphasis on post-critical heat flux regimes, will then follow in Sect. 3.

Pool boiling occurs without an imposed forced flow, where fluid flow is caused by phase change and natural convective only. In external flow boiling, the heated surface may be subject to an imposed fluid flow; however, the fluid field is much larger than the heated surface, and the heat transfer and phase change processes

S. M. Ghiaasiaan (✉)
George W. Woodruff School of Mechanical Engineering, Georgia Institute of Technology, Atlanta, GA, USA
e-mail: mghiaasiaan@gatech.edu

that occur at or near the heated surface have a minimal effect on the properties of the fluid away from the surface. In Sect. 2, the pool boiling curve and boiling regimes are reviewed, followed by a discussion of the phenomenology and theoretical aspects of hysteresis in transition boiling, the minimum film point, and the film boiling regime. Some widely used predictive methods are then presented.

In Sect. 3, the two-phase flow and heat transfer regimes in internal flow boiling in vertical and horizontal flow passages are discussed. Post-critical heat flux heat transfer regimes, including stable film boiling and dispersed droplet film boiling, are then discussed, and widely used predictive methods are presented.

Abbreviations

CHF	Critical heat flux
DNB	Departure from nucleate boiling
LP	Leidenfrost point
MFB	Minimum film boiling
ONB	Onset of nucleate boiling
OSV	Onset of significant void

Nomenclature

A	Atomic number
C, C_p	Specific heat and constant-pressure specific heat (J/kg·K)
D	Diameter (m)
D_H	Hydraulic diameter (m)
F	Time-averaged fraction of the total heated surface that is in contact with liquid; Chen's enhancement factor
G	Mass flux (kg/m ² ·s)
Ga	Galileo number
Gr	Grashof number
\vec{g}	Gravitational acceleration vector (m/s ²)
g	Gravitational constant (= 9.807 m/s ² at sea level)
h	Heat transfer coefficient (W/m ² ·K)
h_{fg}	Latent heat of vaporization (J/kg)
k	Thermal conductivity (W/m·K)
L	Length (m); characteristic length (m)
M	Molar mass (kg/kmol)
Nu	Nusselt number
P	Pressure (N/m ²)
Pr	Prandtl number
q''	Heat flux (W/m ²)
R	Radius (m)
Re	Reynolds number
Re _f	Liquid-only Reynolds number
Re _g	Vapor-only Reynolds number

S	Distance defining intermittency (m); Chen's suppression factor
Sp	Superheat number
Sp^*	Modified superheat number
T	Temperature (K)
t	Time (s)
u, v	Velocity (m/s)
x	Quality
x_{eq}	Equilibrium quality
X_{tt}	Martinelli's factor

Greek Characters

α	Void fraction
α	Thermal diffusivity (m ² /s)
β	Volumetric thermal expansion coefficient (K ⁻¹)
δ	Film thickness (m)
ε	Radiative emissivity
λ_d	Fastest-growing wavelength (m)
λ_{3D}	Wavelength associated with three-dimensional interfacial waves
λ_{KH}	Fastest-growing wavelength for two-dimensional Kelvin–Helmholtz instability (m)
λ_L	Laplace length scale (capillary length) (m)
μ	Viscosity (kg/m·s)
ν	Kinematic viscosity (m ² /s)
θ	Azimuthal angle (rad); angle of inclination with respect to the horizontal plane (rad or degrees)
$\theta_0, \theta_a, \theta_r$	Equilibrium (static), advancing, and receding contact angles (rad or degrees)
ρ	Density (kg/m ³)
σ	Surface tension (N/m)
σ_{SB}	Stefan–Boltzmann constant (5.67×10^{-8} W/m ² ·K ⁴)
τ	Shear stress (N/m ²)

Superscripts

$\bar{\quad}$	Area averaged
*	Calculated at reference temperature

Subscripts

B	Bubble, vapor bulge
cr	Critical
eq	Equilibrium
f	Saturated liquid
FB	Film boiling
Film	Film temperature

FC	Forced convection
g	Saturated vapor
L	Liquid
m	Mixture, mixture average
NB	Nucleate boiling
rad	Radiation
ref	Reference
sat	Saturation
TB	Transition boiling
v	Vapor when it is not at saturation
W	Water
w	Wall
∞	Ambient associated with a large surface

1 Introduction

In this article, transition and film boiling are reviewed. Previously published review articles include Johanssen (1991), Dhir (1991, 1998), as well as textbooks (Collier and Thome 2004; Carey 2008; Ghiaasiaan 2017). Pool boiling refers to the boiling processes without an imposed forced flow, where fluid flow is caused by the phase change process and natural convective phenomena only. In external flow boiling, the heated surface may be subject to an imposed fluid flow; however, the fluid field is much larger than the heated surface, and the heat transfer and phase change processes that occur at or near the heated surface have a minimal effect on the properties of the fluid or the flow field away from the surface. Internal flow boiling occurs in a confined flow field. The heated surface is therefore subject to an imposed flow, and the properties of the fluid are affected by the thermal interaction with the heated surface.

The review will address pool and external flow boiling in section “[Pool Boiling](#).” A discussion of internal flow boiling will then follow in section “[Flow Boiling](#).”

2 Pool Boiling

2.1 The Pool Boiling Regimes and Pool Boiling Curve

The discussion will start with the *pool boiling curve* and *Nukiyama's experiment* (1934). Consider an experiment where a relatively thick electrically heated wire is submerged in a saturated, quiescent liquid pool, where the wire temperature is measured, and the heat flux at the wire surface can be calculated from the supplied electric power. Assume that the liquid and surface constitute a well-wetting pair so

that their static contact angle is about 20° or smaller, the electric power supplied to the heated wire is controlled, and the tests are quasi-steady meaning that each time a new electric power is chosen, the system is allowed to reach steady state before data is recorded. When heat flux, q''_w , is plotted as a function of wall superheat, $\Delta T_w = T_w - T_{sat}$, the “boiling curve” displayed in Fig. 1 results.

The curve suggests at least three different boiling regimes, as shown in Fig. 2, namely, nucleate boiling, transition boiling, and film boiling. Furthermore, the process

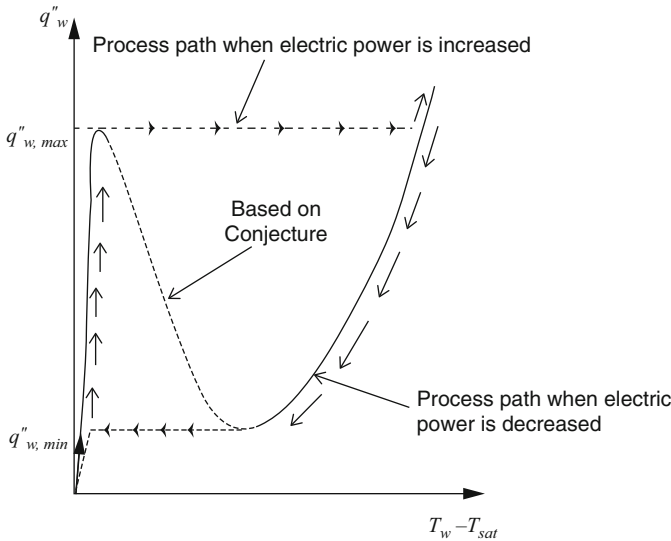
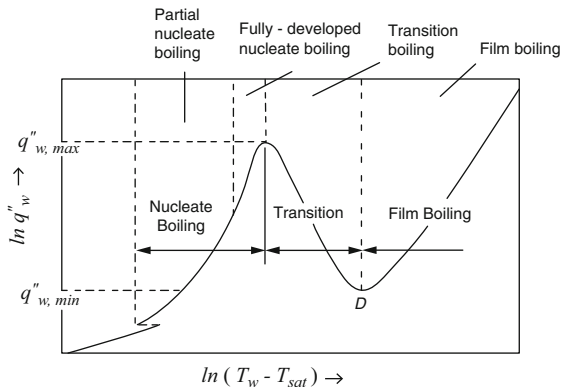


Fig. 1 The pool boiling curve, and process path heat flux is controlled

Fig. 2 Pool boiling regimes



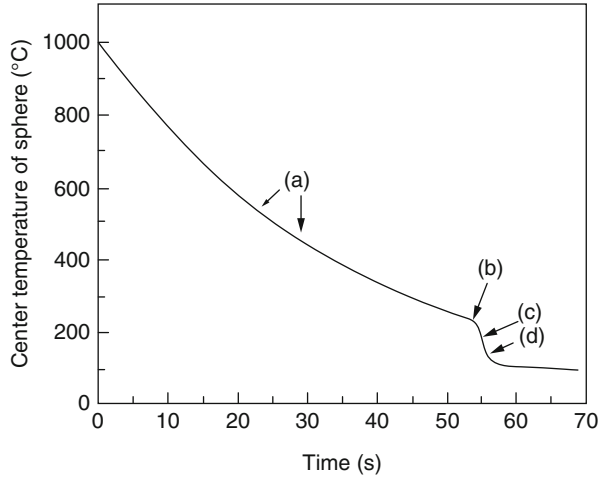
paths for increasing and decreasing electric power (heat flux) are different. For increasing heat flux, the process path would follow the rightward-oriented arrows, and for decreasing power it would follow the leftward-oriented arrows, and the dashed part of the boiling curve is completely bypassed. Based on his experimental data, Nukiyama correctly conjectured that the dashed part of the curve (transition boiling) must be producible when $T_w - T_{\text{sat}}$, rather than q_w'' , is controlled.

Figure 1, as mentioned, will result when the power supplied to the heated element (and thereby the heat flux) is controlled. In an experiment where the heated surface temperature is controlled, however, the entire boiling curve including the transition boiling part can be captured, as shown by the pioneering works of Drew and Mueller (1937) and Berenson (1960). The boiling curve in its entirety can also be observed in quenching experiments. Figure 2 displays the various regimes on a boiling curve.

In the *transition boiling regime*, the heated surface is intermittently dry or in macroscopic contact with liquid. Within the transition boiling region, the local and instantaneous wall surface temperature or heat flux (depending on which one of the two is controlled) fluctuates severely, but on a time- or area-averaged basis, the dry fraction of the heated surface increases as $T_w - T_{\text{sat}}$ is increased. The temperature or heat flux fluctuations are a result of the instability of dry patches that intermittently develop on the heated surface. Beyond the *minimum film boiling point*, MFB (point D), also referred to as the *minimum heat flux* (MHF) point (i.e., to the right of the MFB point in Fig. 2), direct and sustained macroscopic contact between liquid and solid surface does not occur. The heated surface instead remains covered by a vapor film. At the vicinity of the MFB point, however, as will be discussed shortly, sporadic liquid contact with the heated surface takes place.

An alternative to experimentation with an electrically heated specimen that is submerged in a liquid is quenching of a hot specimen by quickly submerging it in liquid. Quenching is a widely used technique in material processing and can occur under accident conditions in water-cooled nuclear reactors and superconductors, as well as during the chill-down of cryogenic liquid transfer systems. In a quenching process, all boiling regimes including transition boiling can occur. For studying the pool and external boiling phenomena, however, often quenching of a relatively small sphere or rodlet is experimentally examined, and during the experiment, the temperature in the quenched object is measured with the objective of obtaining the surface temperature history. The surface temperature can either be directly measured by thermocouples inserted at or near the surface or by the solution of the transient conduction equation in the quenched object and adjusting the surface temperature so that predicted and measured temperatures inside the object agree. These conduction solutions will then provide the heat flux history at the surface, making it possible to construct the boiling curve. Figure 3 displays qualitatively the wall temperature history during a typical quenching process, where the important regimes and boiling regime transition points are also displayed. Quenching experiments are in principle all transient in nature, however, and the data they provide are not representative of quasi-steady-state boiling (the film boiling regime is an exception, however, due to the very slow rate of cooling in that regime).

Fig. 3 Temperature time history during quenching of a 9.5-mm-diameter spherical stainless steel specimen by quickly submerging it in saturated water: (a) stable film boiling, (b) minimum film boiling (*MFB*), (c) critical heat flux (*CHF*), and (d) nucleate boiling (After Kim et al. 2009)



2.2 Boiling Curve Hysteresis

The boiling curves in Figs. 1 and 2 are typical of steady-state experiments with liquid–solid pairs that are well wetting (i.e., the static contact angle for them is not larger than about 20°). Thus, for some common liquids as water, hydrocarbons, and refrigerants boiling on industrial metallic surfaces such as stainless steel or copper, the aforementioned boiling curves are good approximations. These curves do not include some important hysteresis and parametric effects, however.

The first well-documented study of transition boiling was reported by Berenson (1962) who performed experiments using n-pentane and carbon tetrachloride on a horizontal disk that was heated from beneath by condensing water. Berenson's observations confirmed that nucleate and film boiling mechanisms both contribute to the heat transfer process in transition boiling.

Hysteresis in transition boiling is among the most important and not yet fully resolved issues about the boiling curve. Witte and Lienhard (1982) noted that the surface wettability was likely to play an important role in this hysteresis. By examining a variety of experimental pool boiling data, Witte and Lienhard (1982) showed that the transition boiling line was in general not unique, and two distinct transition boiling curves may be obtained for a liquid–solid combination depending on whether the transition boiling region is approached from the nucleate boiling part by increasing the surface temperature or from the film boiling region by reducing the surface temperature. By recreating the aforementioned experiments of Berenson (1962), Ramillison and Lienhard (1987) confirmed the occurrence of hysteresis, as well as a clear dependence of the transition boiling curves on static contact angle, as shown in Fig. 4. An important point about the experiments of Ramillison and Lienhard (1987) is the wide range of contact angles and the significant difference between advancing and receding contact angles (contact angle hysteresis) for the three fluids that are depicted in

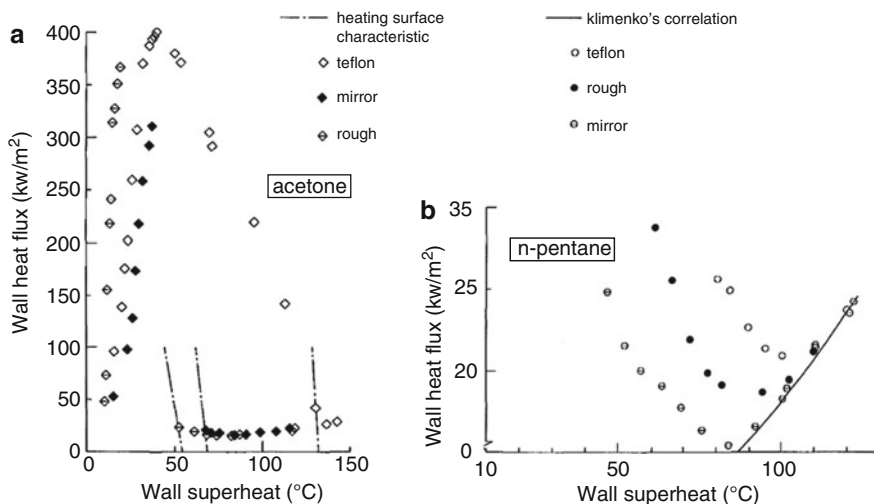


Fig. 4 Boiling curve hysteresis in the experiments of Ramilison and Lienhard (1987): (a) boiling curve for acetone boiling on Teflon-coated, mirror-finished, and rough surfaces when transition boiling regime is approached starting from nucleate boiling regime; (b) film transition and transition boiling curves for n-pentane on Teflon-coated, mirror-finished, and rough surfaces when transition boiling region is approached starting from film boiling regime

Fig. 4a, b. For example, for the temperatures in their experiments, Ramilison and Lienhard (1987) reported that $\theta_r \approx 0$ and $\theta_a \approx 5^\circ$ (i.e., near perfect surface wetting) for acetone on a Teflon-coated surface, and for n-pentane $\theta_r \approx 8, 10, 15^\circ$ and $\theta_a \approx 24, 35, 45^\circ$ with Teflon-coated, mirror-finished, and rough surfaces, respectively.

Bui and Dhir (1985a) performed experiments on a vertical surface and confirmed that different transition boiling curves could be obtained depending on the side of the boiling curve from which the transition boiling part of the curve was approached (i.e., the nucleate boiling side or the film boiling side). Based on experiments with a vertical copper plate, Bui and Dhir (1985a), and later Liaw and Dhir (1986), showed that the magnitude of hysteresis in the transition boiling depends on the static contact angle.

For clarity, the simplified generic pool boiling curves depicted in Fig. 5 will be used for discussion, and it is assumed that the advancing and receding contact angles are different, i.e., $\theta_a > \theta_0 > \theta_r$. This figure qualitatively shows the hysteresis in transition boiling. If the transition boiling curve is obtained by starting from the film boiling part of the curve and reducing the wall superheat, the boiling curve will follow the line d-e-f-g. The heat flux–wall superheat curve deviates from the pure film boiling curve before it reaches the minimum heat flux point, and with further reduction in wall superheat, the gradient of the heat flux–wall superheat curve becomes negative. The part of the boiling curve between points e and MFB, i.e., where the curve deviates from the film boiling line, but the heat flux is larger than the minimum heat flux and the wall superheat is larger than the wall superheat at the

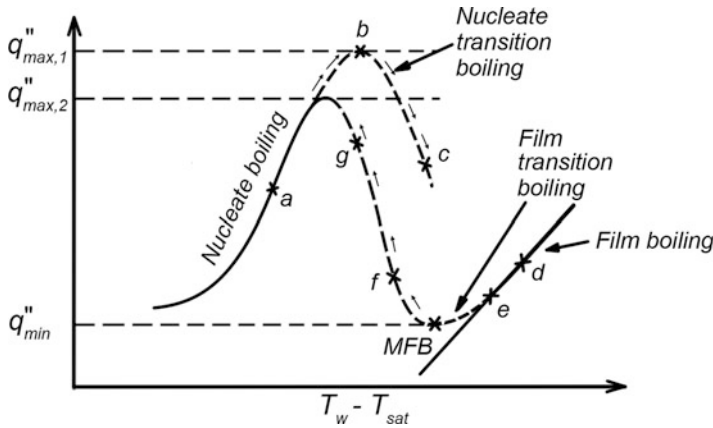


Fig. 5 Hysteresis in the transition boiling regime for a liquid–solid pair with significantly different contact angle hysteresis

minimum film boiling point, has been named film–transition boiling (Ramilison and Lienhard 1987). During film boiling, as will be explained later, a vapor film separates the heated surface from liquid. Hydrodynamic waves form on the liquid–vapor interphase and play an important role in the phenomenology of film boiling. While in the film boiling zone (i.e., for points to the right of point *e* in Fig. 5) there is virtually no liquid–surface direct contact, in the film–transition boiling region, some liquid–surface contact takes place near the nodes of the waves that form at the vapor–liquid interphase in film boiling. As the wall superheat is reduced and the transition boiling part of the boiling curve is reached, the area patches covered by liquid increase in extent and number, and film boiling occurs on the part of the surface covered by vapor, while nucleate boiling takes place on areas covered by liquid. The expansion of the surface patches that are covered by liquid evidently involves the advancing contact angle. Thus, when the transition boiling region is approached from the film boiling side, one may assume that the contact angle in effect is close to θ_a .

If the transition boiling zone of the boiling curve is approached from the nucleate boiling side by increasing the surface temperature (recall that the transition boiling part of the curve can only be obtained in steady-state experiments if the surface temperature is controlled), the boiling curve will follow the *a*–*b*–*c* line. The peak heat flux ($q''_{\max,1}$ in Fig. 5) and the surface temperature at which the peak heat flux occurs surpass the peak heat flux ($q''_{\max,2}$ in Fig. 5) and the peak heat flux temperature, respectively, which are measured when the transition boiling curve is obtained by starting from the film boiling regime and reducing the wall superheat. The phenomenology that leads to this apparent surpassing of CHF can be understood by remembering that at and beyond the peak heat flux, the dry patches that occur on the heated surface tend to expand at the expense of the liquid that is in contact with the wall. The dry patches support an essentially film boiling regime, while the areas covered by liquid support fully developed nucleate boiling representative of the

Zone III regime in Fig. 2. The process is thus likely to involve a receding contact angle, and when $\theta_r < \theta_a$, the situation is similar to boiling on a surface with better wettability. Better wettability, equivalent to smaller contact angle, helps the spreading of the liquid film which is followed by vigorous bubble nucleation and the blowing away of the liquid. The fully developed nucleate boiling (i.e., the boiling regime in Zone III of Fig. 2) is thus extended beyond the CHF point at least for some portion of the heated surface. The heat transfer regime on the transition boiling curve near the peak heat flux point is a combination of film boiling and fully developed nucleate boiling and is often called the nucleate–transition boiling (Ramilison and Lienhard 1987). Ramilison and Lienhard noted that no hysteresis in transition boiling occurred in experiments with acetone boiling on a Teflon-coated surface, where near-perfect wetting took place.

The existence of the aforementioned hysteresis in transition boiling under steady-state conditions has been disputed by some researchers, however. Experimental studies by Auracher and coworkers (Blum et al. 1996; Hohl et al. 2001; Auracher and Marquardt 2002) and Ohtaki and Koizumi (2006), for example, have shown no hysteresis when the experiments are performed in true steady state, and the heated surface is maintained clean. Figures 6 and 7 show pool boiling curves for FC-72

Fig. 6 Steady-state boiling curve of FC-72 on a copper-heated disk ($P = 0.13\text{MPa}$) (Auracher and Buchholz 2005)

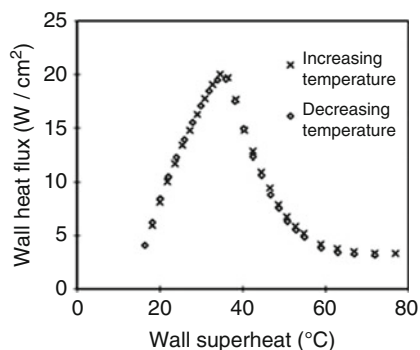
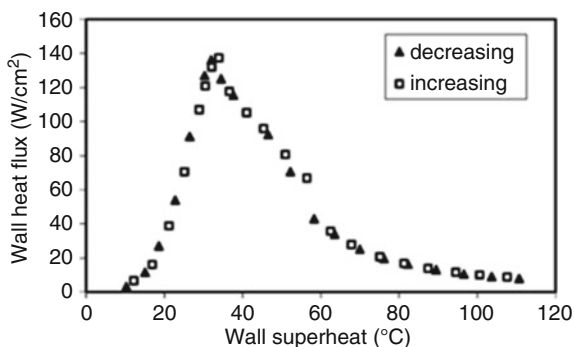


Fig. 7 Steady-state boiling curve of water on a copper-heated disk ($P = 0.99\text{bars}$) (Auracher and Marquardt 2002)



boiling on a copper-heated block electroplated with a 20-micron-thick nickel layer and distilled water boiling on a copper-heated disk electroplated with a 50-micron-thick nickel layer, respectively. The wall temperature was controlled by comparing the measured temperature close to the boiling surface with a set point value and using the difference in a controller for adjusting the power of the electric heating system. In this way, carefully controlled steady-state or transient experiments could be performed. The experiments depicted in Figs. 6 and 7 were thus performed under true steady-state conditions, with clean heated surfaces. The FC-72 and nickel pair represent a well-wetting condition with a small contact angle, while water and nickel represent a partially wetting pair ($\theta_a \approx 79^\circ$, $\theta_r \approx 34^\circ$, Faghri and Zhang 2006). No hysteresis can be observed in these figures and other similar tests. However, in transient experiments hysteresis can be observed in most parts of the boiling curve. Figures 8 and 9 show clearly the important effect of transient experimentation on the boiling curve. Auracher and Marquardt (2002) argue that boiling curves measured under steady-state conditions with a proper control and a clean heater surface do not exhibit a hysteresis in the transition boiling region. The hysteresis resulting from transient heating and cooling in transition boiling had been noted earlier by Bui and Dhir (1985a), as shown in Fig. 10.

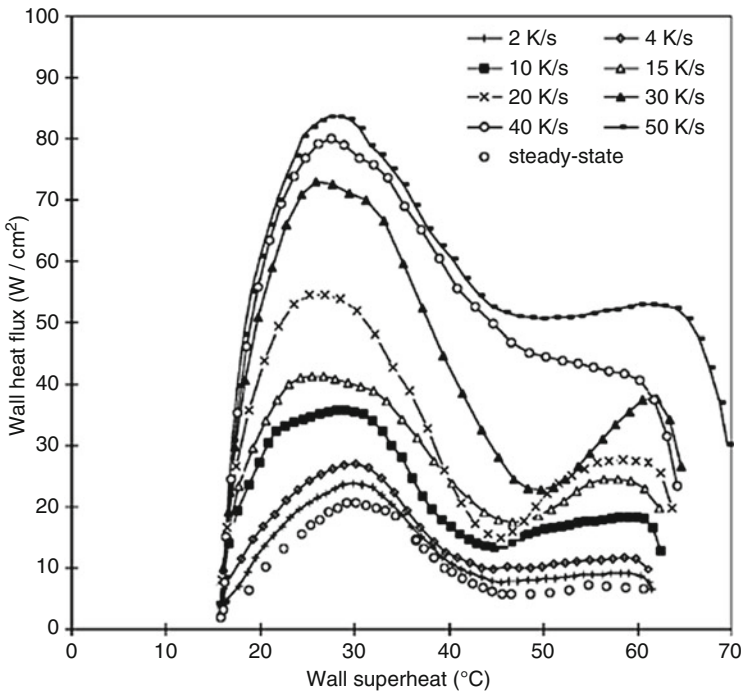


Fig. 8 Boiling curves for FC-72 during transient heating experiments ($P = 0.13\text{MPa}$) (Hohl et al. 2001)

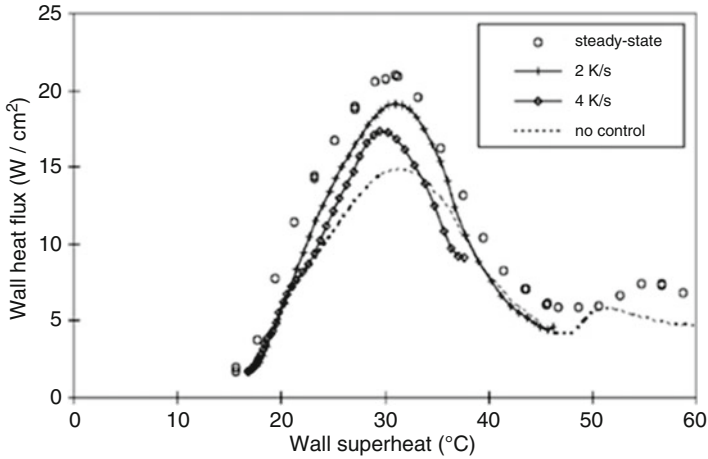
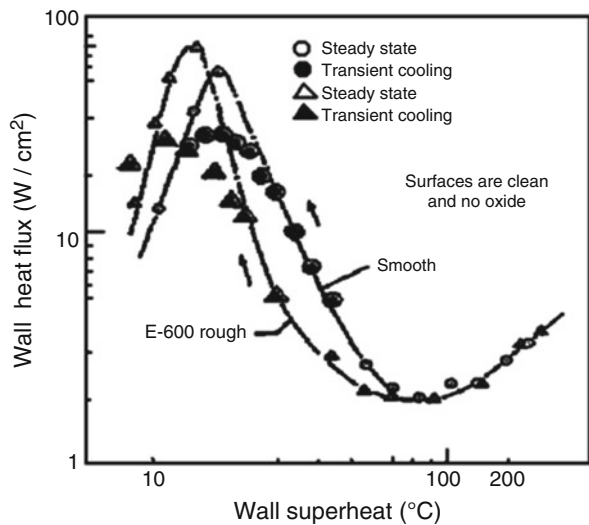


Fig. 9 Boiling curves for FC-72 during transient heating experiments ($P = 0.13\text{MPa}$) (Hohl et al. 2001)

Fig. 10 Boiling curves in steady-state and transient experiments for water boiling on a vertical copper surface (Bui and Dhir 1985a; Dhir 1991)



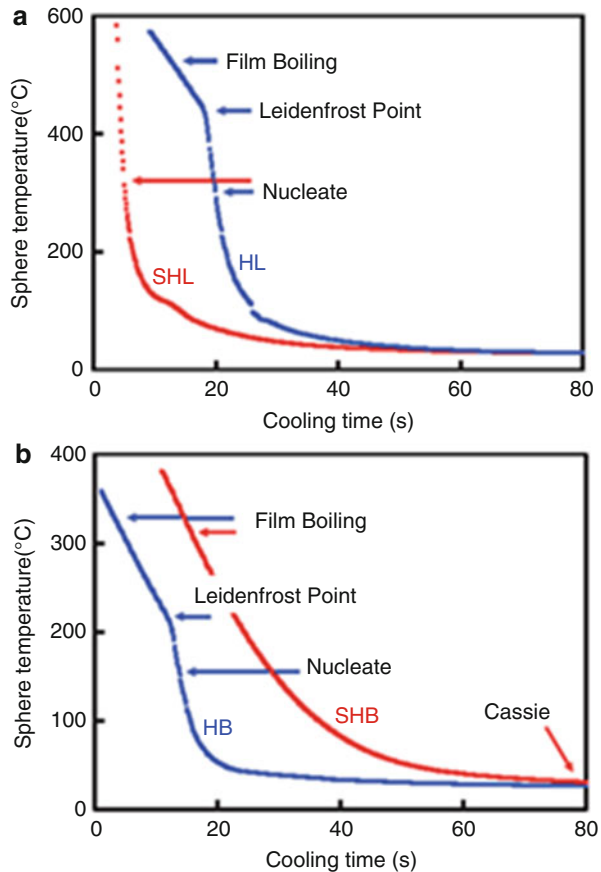
Further evidence questioning the occurrence of hysteresis in steady-state conditions has been provided by Ohtaki and Koizumi (2006), who performed experiments with water, using the top surface of a large and thick copper block ($15 \times 15 \text{ mm}^2$ area and 60 mm thick) to ensure that due to the large thermal capacity of the block, the temperature of the block remained in a time-smoothed steady state. They did not observe hysteresis in the transition boiling regime.

2.3 Parametric Effects

Some important parametric effects on the pool boiling curve, in particular with respect to the transition and film boiling regimes, are now discussed. The discussion will address CHF and nucleate boiling as well, as these regimes are directly relevant to the transition boiling regime and its range of occurrence.

The effect of surface wettability with respect to the transition boiling as well as CHF and MFB points has already been discussed. In nucleate boiling, better wettability (smaller contact angle) leads to smaller bubble departure diameter but higher bubble departure frequency. Moreover, increased surface wettability shifts the nucleate boiling line toward the right. Thus, with increased surface wettability, decreasing nucleate boiling heat transfer coefficients (for the same $T_w - T_{sat}$) are obtained. Increased surface wettability also increases the maximum heat flux as well as the minimum film boiling temperature (Roy Chowdhury and Winterton 1985; Liaw and Dhir 1986). Figure 11 depicts the results of quenching experiments of Vakarelski et al. (2012). In these experiments 20-mm-diameter stainless steel

Fig. 11 Sphere temperature versus cooling time for 20-mm steel spheres held in water at 22 °C in the experiments of Vakarelski et al. (2012). (a) Superhydrophilic sphere (SHL) (contact angle $<10^\circ$) and hydrophilic sphere (HL) (contact angle $\sim 30^\circ$). (b) Hydrophobic sphere (HB) (contact angle $\sim 100^\circ$) and superhydrophobic surface sphere (SHB) (contact angle $>160^\circ$)



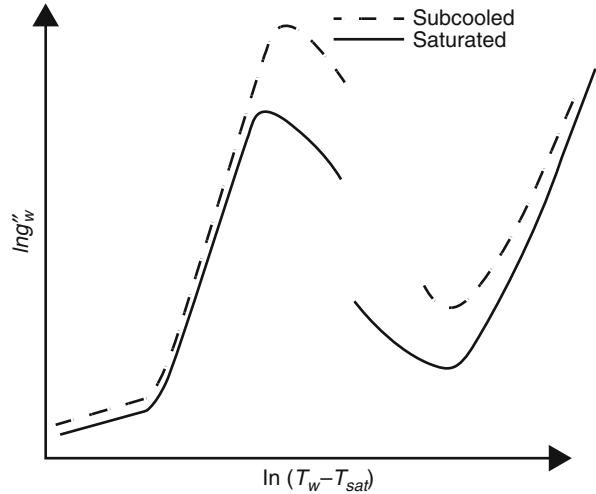
spheres, with their surfaces modified in order to obtain various levels of hydrophobicity, were quenched in water. The surface conditions included smooth hydrophilic produced by cleaning with organic reagents, smooth hydrophobic produced by silanization with trichloro(1H,1H,2H,2H-perfluorooctyl)silane, textured superhydrophobic produced by treatment with a commercial superhydrophobic coating agent, and textured superhydrophilic produced by plasma cleaning of the surfaces previously treated with the superhydrophobic agent. For the superhydrophilic (SHL) sphere, the maximum temperature was not high enough to initiate film boiling. For hydrophilic (HL) ($\theta_0 \approx 30^\circ$) and hydrophobic (HB) ($\theta_0 \approx 100^\circ$) spheres, the film boiling mode on the surface ended with the collapse of the vapor layer and an explosive release of bubbles (Fig. 11). However, for the superhydrophobic (SHB) sphere ($\theta_0 \approx 160^\circ$), no vapor-layer collapse was observed. Film boiling remained stable throughout the boiling process. Nucleate boiling, CHF, and transition boiling regimes were completely bypassed, and film boiling remained stable until the surface was sufficiently cooled so that liquid–surface contact was established without bubble nucleation. For the superhydrophobic (SHB) surface case, the film boiling was replaced with the Cassie-state liquid–surface contact. (The Cassie or Cassie–Baxter state refers to conditions where liquid resides on a rough surface without completely penetrating the surface grooves and has been named after Cassie and Baxter (1944) who modeled the contact angle on composite surfaces and surfaces with microgrooves. A useful discussion can be found in Gopalan and Kandlikar (2014)). Similar conclusions were arrived at more recently by Fan et al. (2016) based on quenching experiments with subcooled water.

The hydrophobicity of surfaces can be manipulated by the deposition of nanoparticle films (nanocoating) (Kim et al. 2002; Hwang and Kaviany 2006; Forrest et al. 2010). By applying a layer-by-layer assembly method using polymer/SiO₂ nanoparticle layers deposited on nickel wires and stainless steel plates, Forrest et al. (2010) could obtain static contact angles with water in the range of 3–141°. The critical heat flux and nucleate boiling heat flux (the latter for given wall superheats) both monotonically improved with better wettability and up to 100% improvement in CHF and better than 100% improvement in the nucleate boiling heat flux were obtained.

Increased surface roughness tends to move the nucleate and transition lines to the left, implying improvement in the nucleate boiling heat transfer characteristics. Figure 10 depicts the data of Bui and Dhir (1985a). In the aforementioned experiments of Ohtaki and Koizumi (2006), surface roughness effect in transition boiling was small, however. Surface roughness also affects the minimum film boiling, as will be discussed later. The effect of surface roughness on heat transfer in stable film boiling is small and is primarily due to increased surface area and the change in surface radiative emissivity. Surface contamination (deposition and oxidation) and improved surface wettability both move the nucleate boiling part of the boiling curve to the right, i.e., a higher wall superheat will be needed for any given heat flux.

Liquid pool subcooling improves heat transfer in all boiling regimes, as shown qualitatively in Fig. 12, except for the fully developed nucleate boiling region where its effect is small due to the overwhelming contribution of bubble generation (i.e., phase change) to heat transfer in comparison with convection. Nucleate boiling is the preferred

Fig. 12 The effect of liquid pool subcooling on the boiling curve



mode of heat transfer for many thermal cooling systems, since it can sustain large heat fluxes with low heated surface temperatures. Furthermore, in the transition boiling, a fraction of the surface is subject to a heat transfer regime similar to fully developed nucleate boiling. In the fully developed nucleate boiling zone (the slugs and jet zones), the heat transfer coefficient is insensitive to surface orientation. In the partial nucleate boiling zone, however, heat transfer is affected by orientation.

2.4 Film Boiling

Hydrodynamic models with minor adjustments have done well in predicting the pool film boiling heat transfer in many situations. Film boiling models and correlations for some important heated surface configurations are now reviewed.

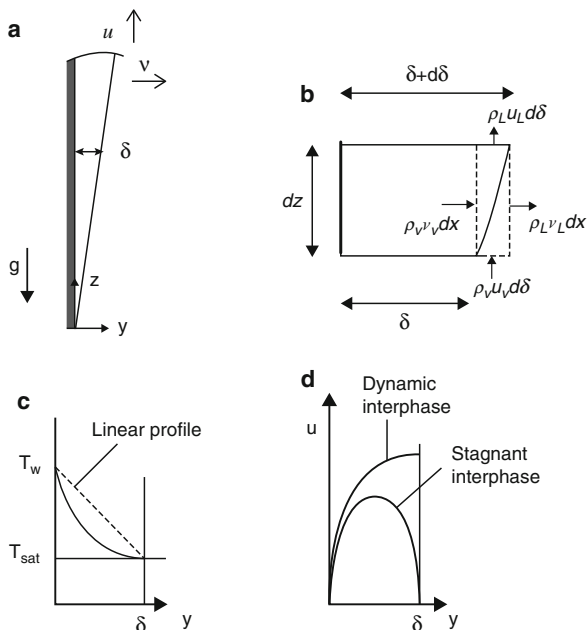
2.4.1 Film Boiling on Vertical Flat Surfaces

Film boiling on a vertical and flat surface is among the simplest film boiling configurations and can be solved analytically, provided that the vapor film remains laminar, coherent, and smooth-surfaced. These assumptions are not always realistic, and their effects will be discussed later. However, as will be shown, the solutions for the idealized vapor film can be modified in order to compensate for some of these unrealistic assumptions.

Coherent and Laminar Film with Smooth Vapor–Liquid Interface

Figure 13a depicts the configuration of the vapor film, which flows upward on the vertical surface, and its thickness grows due to evaporation as it rises. The following assumptions are made: (a) the process is steady state; (b) the liquid and vapor are incompressible; (c) the vapor film is laminar; (d) the liquid is infinitely large and except for the flow that is caused by thermal and momentum interaction with the

Fig. 13 Idealize laminar film boiling on a vertical heated surface: (a) film configuration, (b) an infinitesimally thin slice, (c) temperature profiles, and (d) velocity boundary conditions at liquid–vapor interface



rising vapor film, the liquid is stagnant; (e) when the liquid is subcooled, natural convection takes place in the liquid as a result of liquid temperature variation caused by thermal interaction with the vapor film, and Boussinesq approximation can be applied for the liquid; (f) the flow field is two dimensional; (g) radiation heat transfer effects are negligible in the liquid; and (h) the thermophysical properties are constant. The mass, momentum, and energy conservation equations for the vapor phase will then be

$$\frac{\partial u_v}{\partial z} + \frac{\partial v_v}{\partial y} = 0 \tag{1}$$

$$u_v \frac{\partial u_v}{\partial z} + v_v \frac{\partial u_v}{\partial y} = \nu_v \frac{\partial^2 u_v}{\partial y^2} + \frac{g(\rho_L - \rho_v)}{\rho_v} \tag{2}$$

$$u_v \frac{\partial T_v}{\partial z} + v_v \frac{\partial T_v}{\partial y} = \alpha_v \frac{\partial^2 T_v}{\partial y^2} \tag{3}$$

The mass, momentum, and energy conservation equations for the liquid phase will then be

$$\frac{\partial u_L}{\partial z} + \frac{\partial v_L}{\partial y} = 0 \tag{4}$$

$$u_L \frac{\partial u_L}{\partial z} + v_L \frac{\partial u_L}{\partial y} = v_v \frac{\partial^2 u_L}{\partial y^2} + g\beta_L(T_L - T_{L,\infty}) \quad (5)$$

$$u_L \frac{\partial T_L}{\partial z} + v_L \frac{\partial T_L}{\partial y} = \alpha_L \frac{\partial^2 T_L}{\partial y^2} \quad (6)$$

The boundary conditions for these equations are

At $y = 0$

$$u_v = v_v = 0 \quad T_v = T_w \quad (7)$$

At $y \rightarrow \infty$

$$u_L = v_L = 0, T_L = T_{L,\infty} \quad (8)$$

At $y = \delta$

$$u_v = u_L, T_v = T_L = T_{\text{sat}}(P) \quad (9)$$

$$\rho_g \left[v_v - u_v \frac{d\delta}{dz} \right] = \rho_f \left[v_L - u_L \frac{d\delta}{dz} \right] \quad (10)$$

$$\mu_f \frac{\partial u_L}{\partial y} = \mu_g \frac{\partial u_v}{\partial y} \quad (11)$$

$$-k_g \frac{\partial T_v}{\partial y} + q''_{\text{rad}} = -\rho_g \left[v_v - u_v \frac{d\delta}{dz} \right] h_{fg} - k_f \frac{\partial T_L}{\partial y} \quad (12)$$

where q''_{rad} is the radiative heat flux from the wall to the liquid–vapor interphase. Note that Eq. 10 can be derived by performing a mass balance on the control volume depicted in Fig. 13b.

The above equations can be simplified if the liquid is saturated and radiation effect is neglected. In this case, $T_L = T_{\text{sat}}(P)$ everywhere, Eq. 6 will be redundant, and Eq. 5 will simplify to

$$u_L \frac{\partial u_L}{\partial z} + v_L \frac{\partial u_L}{\partial y} = v \frac{\partial^2 u_L}{\partial y^2} \quad (13)$$

Also, neglecting the effect of superheating of the vapor, Eq. 12 can be replaced with

$$-k_g \left(\frac{\partial T_v}{\partial y} \right)_{y=\delta} = h_{fg} \frac{d}{dz} \left[\rho_v \int_0^\delta u_v(y) dy \right] \quad (14)$$

Koh (1962) derived a similarity solution for the above-simplified set of equations and showed that the behavior of the vapor film as well as the heat transfer process depends on the vapor Prandtl number, Pr_v , and the forthcoming two dimensionless parameters:

$$\frac{C_{Pv}(T_w - T_{sat})}{h_{fg}Pr_v} \quad (15)$$

$$[(\rho_v\mu_v)/(\rho_L\mu_L)]^{1/2} \quad (16)$$

Parametric calculations by Koh (1962) showed that interfacial shear is important except for vanishingly small values of $[(\rho_v\mu_v)/(\rho_L\mu_L)]^{1/2}$. The parametric calculations also indicated that the temperature profile across the film is approximately linear only when the film is very thin and becomes increasingly nonlinear as the film thickness increases.

The vapor film momentum equation can be significantly simplified by bearing in mind that the vapor film that forms on a vertical wall tends to rise because of buoyancy, much like the boundary layer that forms on vertical surfaces during free convection, and in most cases, the inertia of the vapor is insignificant. The left side of Eq. 2 will then vanish, and Eq. 2 reduces to

$$\mu_v \frac{d^2 u_v}{dy^2} + g(\rho_L - \rho_v) = 0. \quad (17)$$

For a contiguous laminar film with a smooth surface rising in stagnant liquid in steady state, the boundary conditions for this equation are

$$u_v = 0 \text{ at } y = 0 \quad (18)$$

$$u_v = 0 \text{ at } y = \delta \text{ for the stagnant interphase (i.e., no-slip),} \quad (19)$$

$$\frac{du_v}{dy} = 0 \text{ at } y = \delta \text{ for the dynamic interphase (i.e., zero shear stress)} \quad (20)$$

Either of the assumed boundary conditions at $y = \delta$ decouples the momentum equation of the vapor film from the liquid (see Fig. 13d). The vapor film can then be modeled by using the integral technique, described in standard heat transfer textbooks (see, e.g., Ghiaasiaan (2011)). Bromley (1950) performed such analysis. The solution of Eq. 17 with these boundary conditions gives the velocity profile in the vapor film:

$$u_v(y) = \frac{g\Delta\rho}{2\mu_v} [C_1\delta y - y^2] \quad (21)$$

where $C_1 = 1$ for the stagnant interphase, and $C_1 = 2$ for the dynamic interphase. If it is assumed that the temperature profile across the vapor film is linear, Eq. 14 gives

$$h_{fg} \frac{d}{dz} \left[\rho_v \int_0^{\delta} u_v(y) dy \right] = k_v \frac{T_w - T_{sat}}{\delta} \quad (22)$$

One can now combine Eqs. 21 and 22, to derive a differential equation for δ . The solution of the latter differential equation leads to

$$\delta = \left[\frac{8}{3(C_1/2 - 1/3)} \frac{k_v(T_w - T_{sat})\mu_v z}{\rho_v h_{fg} g \Delta \rho} \right]^{1/4} \quad (23)$$

Knowing δ , and assuming a linear temperature distribution across the vapor film, one can calculate the local film boiling heat transfer coefficient from $h_{FB} = k_v/\delta$. The average heat transfer coefficient for a vertical surface of length L can then be found from $\bar{h}_{FB} = \frac{1}{L} \int_0^L h dz$, and this integration yields (Bromley 1950)

$$\bar{h}_{FB} = C \left[\frac{\rho_v h_{fg} g \Delta \rho k_v^3}{(T_w - T_{sat}) \mu_v L} \right]^{1/4} \quad (24)$$

where $C = 0.663$ for the stagnant interphase and $C = 0.943$ for the dynamic interphase. The stagnant interphase is evidently appropriate when the liquid viscous resistance is much larger than the vapor viscous resistance. This condition holds when $[(\rho_v \mu_v)/(\rho_L \mu_L)]^{1/2} \ll 1$ (Koh 1962), which is often the case for film boiling in a quiescent liquid pool.

The derivation thus far has neglected the occurrence of superheating in the vapor film. Some of the heat transferred from the wall to the flow field is used up for superheating of the vapor film. To account for the vapor superheat, Eq. 22 should be simply modified according to

$$h_{fg} \frac{d}{dz} \left[\rho_v \int_0^{\delta} u_v(y) dy + \rho_v C_{Pv} \int_0^{\delta} u_v(y) \frac{T_v - T_{sat}}{h_{fg}} dy \right] = -k_v \left(\frac{\partial T_v}{\partial y} \right)_{y=0} \quad (25)$$

For an assumed linear temperature profile in the vapor film, when thermophysical properties of vapor are assumed to be constant, the right side of Eq. 25 will be the same as the right side of Eq. 22. The solution of the aforementioned problem with Eq. 25 leads to Eq. 24 provided that h_{fg} is replaced with h'_{fg} where

$$h'_{fg} = h_{fg} \left[1 + C_1 \frac{C_{Pv}(T_w - T_{sat})}{h_{fg}} \right] \quad (26)$$

where the value of the constant C_1 depends on the temperature profile in the film. A value of 0.5 was suggested by Bromley (1950), but a value of 0.34 has been found to agree with data (Hsu and Graham 1986).

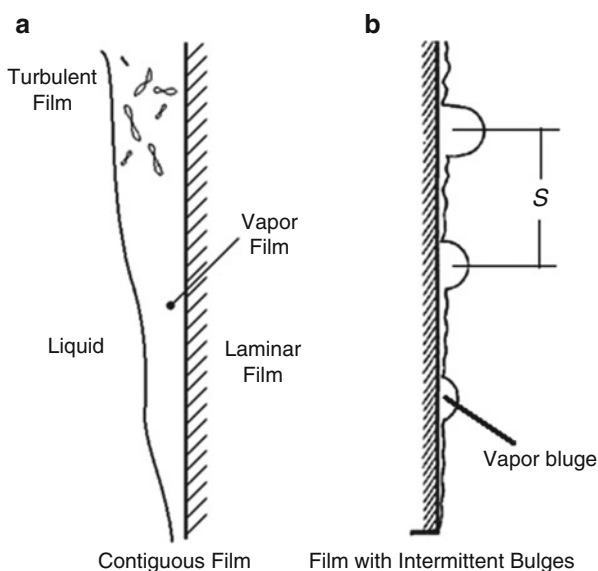
The above derivations for a laminar and coherent vapor film with smooth interface can be applied to inclined surfaces provided that g is replaced with $g \sin \theta$, with θ representing the angle of inclination with respect to the horizontal plane.

Effects of Turbulence and Interfacial Waves

Experiments have shown that Eq. 24 is only valid for short vertical surfaces and underpredicts experimental data for long surfaces. For boiling of water, for example, Eq. 24 underpredicts measurements when the length of the heated vertical surface is more than about one-half inch (Hsu and Graham 1986). One reason could be the assumption of laminar film. The vapor film, if it remains contiguous and coherent, will grow in thickness and eventually become turbulent (see Fig. 14a). Hsu and Westwater (1960) performed an analysis similar to Bromley's, but they assumed that: (a) the vapor film would become turbulent for $\delta \sqrt{\frac{\tau_w/\rho_v}{\nu_v}} > 10$, (b) the entire thermal resistance of the vapor film occurred in the vapor film's viscous sublayer, and (c) the temperature profile in the viscous sublayer was linear. Hsu and Westwater compared their model with data representing five different fluids boiling on the outside of vertical tubes with 5–16 cm heights and noted that the data could be predicted within $\pm 32\%$.

The most serious shortcoming of Eq. 24, however, is that it does not account for the intermittency of the vapor film. Experimental observations show that the vapor film on long, heated surfaces does not remain smooth and coherent. Interfacial waves develop, and the vapor film becomes intermittent before the film grows sufficiently

Fig. 14 Film boiling on a long, vertical surface



thick to turn turbulent. Based on experimental observations, Bailey (1971) suggested that the vapor film supports a spatially intermittent structure. At the bottom of each spatial interval, the vapor film is initiated and grows, until it becomes unstable and eventually is disrupted by the time it reaches the top of the interval. Following its disruption, a fresh film is initiated in the next interval. The vapor film remains laminar in the aforementioned intervals. Based on the argument that the intermittency results from hydrodynamic instability, Leonard et al. (1978) proposed that for vertical surfaces, L in Eq. 24 should be replaced with $S \approx \lambda_{cr} = 2\pi \sqrt{\frac{\sigma}{g\Delta\rho}}$, with λ_{cr} representing the critical (neutral) wavelength according to the two-dimensional Rayleigh–Taylor instability (for a discussion of linear instability analysis of interfacial waves that are of interest in boiling, see Ghiaasiaan (2017)). With this substitution, the *modified Bromley correlation* is obtained, which agrees with inverted annular film boiling data in vertical tubes (Hsu and Graham 1986).

Bui and Dhir (1985a) studied subcooled and saturated film boiling of atmospheric water on a vertical surface. Their visual observations showed an intermittent, but considerably more complicated, vapor film behavior. In low subcooling experiments, three-dimensional waves with large and small amplitudes developed on the vapor–liquid interface (Fig. 14b). The amplitude of the large waves was of the order of a few centimeters and grew with distance from the heated surface leading edge. The peaks of the three-dimensional waves evolved into bulges that resembled bubbles which were attached to the surface, and their height was one or two orders of magnitude larger than the thickness of the surrounding vapor film. The bulges acted as vapor sinks for the vapor flowing in the film and grew in size as they moved upward due to buoyancy. The local heat transfer coefficient was highly transient as a result of intermittent exposure to vapor film and vapor bulges. The vapor path was thus interrupted rendering the distance between two adjacent bulges to be the effective average vapor path length, in agreement with the aforementioned vapor film intermittency argument. Waves with small and large amplitudes, and intermittency with respect to film hydrodynamics as well as heat transfer, were also noted in experiments dealing with subcooled film boiling on vertical surfaces (Vijaykumar and Dhir 1992a, b). The local liquid-side heat flux varied along the film and the bulge and had its maximum at the wave peaks (i.e., on the bulges). Based on these observations, Bui and Dhir (1985b) developed a mechanistic model that separately accounts for heat transfer between the surface and the liquid phase through the vapor film and the bulges and assumes that the bulges are separated by the wavelength of three-dimensional waves that form on the vapor–liquid interface. This wavelength was obtained to be

$$\lambda_{3D} \approx \sqrt{2}\lambda_d \quad (27)$$

where λ_d is the two-dimensional interfacial fastest-growing wavelengths. Bui and Dhir calculated λ_d using a linear two-dimensional instability analysis (Bui 1984).

A more recent predictive method for film boiling on flat and long vertical surfaces has been proposed by Nishio and Ohtake (1993). For saturated film boiling, and

using the integral method analysis of Nishio and Ohtake (1992) for film boiling on a vertical surface in subcooled liquid, they showed that when $\rho_g/\rho_f \ll 1$, the most dangerous (the fastest-growing) wavelength for two-dimensional Kelvin–Helmholtz instability, λ_{KH} , can be found from

$$\lambda_{KH} = 16.2 \left[\frac{\text{Pr}_{v, \text{film}}^3}{Sp^* Gr_g \lambda_L} \right]^{1/11} \quad (28)$$

where $\lambda_L = \sqrt{\frac{\sigma}{g(\rho_f - \rho_g)}}$ is the Laplace length scale, and the superheat and modified superheat numbers, Sp and Sp^* , respectively, are defined as

$$Sp = \frac{C_{Pv}(T_w - T_{\text{sat}})}{h_{fg}} \quad (29)$$

$$Sp^* = \frac{Sp}{1 + Sp/2} \quad (30)$$

Using the aforementioned λ_{KH} as the length scale representing the intermittency of the vapor film, Nishio and Ohtake (1993) proposed the following correlations for the average heat transfer coefficient. For film boiling in saturated liquid:

$$\overline{Nu}_{\lambda_{KH}} = \frac{\overline{h}_{FB} \lambda_{KH}}{k_v} = 0.74 \left[\frac{Gr_{g, \lambda_{KH}} \text{Pr}_{v, f}}{Sp^*} \right]^{1/4} \quad (31)$$

where the $Gr_{g, \lambda_{KH}}$ represents Grashof number defined by using λ_{KH} as the length scale:

$$Gr_{g, \lambda_{KH}} = \frac{g[(\rho_{L, \text{film}} - \rho_v)/\rho_v] \lambda_{KH}^3}{\nu_v^2} \quad (32)$$

For film boiling in a subcooled liquid, Nishio and Ohtake (1993) proposed

$$\begin{aligned} \overline{h}_{FB} &= \overline{h}_{FB, \text{sat}} \\ &+ 0.067 \left(\frac{k_v}{\lambda_{KH}} \right) \left[\frac{\text{Pr}_{L, \text{film}}^{0.21}}{(\rho_g/\rho_f)(\mu_g/\mu_f)^{0.23}} \right] (Gr_{g, \lambda_{KH}} \text{Pr}_{L, \text{film}})^{1/4} \frac{T_{\text{sat}} - T_L}{T_w - T_{\text{sat}}} \quad (33) \end{aligned}$$

In the above expressions, subscripts “ L , $film$ ” represent the liquid-phase film temperature. Vapor properties (properties with subscript v) should also be calculated at vapor film temperature.

It should be noted that when a vertical surface is not flat, the analyses presented here apply as long as the vapor film thickness is much smaller than the principle radii

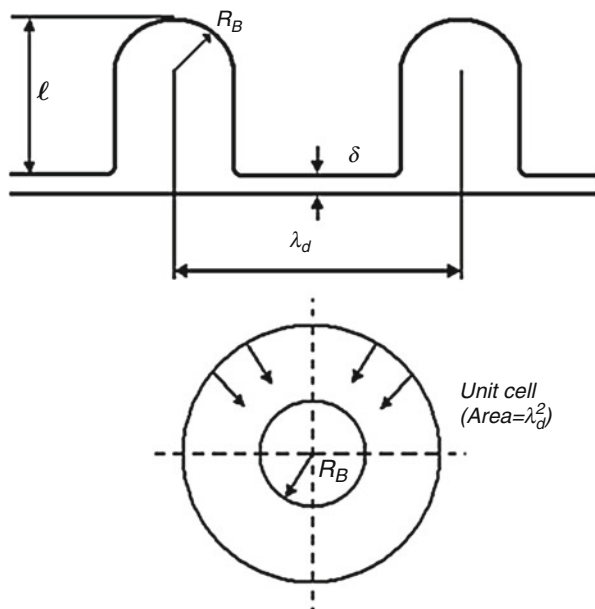
of curvature of the surface. This condition is satisfied in many important applications (e.g., in the vertical rod bundles of nuclear reactor cores and the vertical tube bundles of steam generators). Also, film boiling on moderately inclined flat surfaces can be treated by using vertical flat surface methods, provided that the gravitational constant g in the correlations is replaced with $g \sin \theta$, with θ representing the angle with the horizontal plane.

2.4.2 Film Boiling on a Horizontal, Flat Surface

A coherent and wavy vapor film separates the heated surface from the overlying liquid in this case, and the vapor film is periodically disrupted in order to eject a vapor bubble. Models based on these observations have been proposed by Chang (1959), Berenson (1961), Hamil and Baumeister (1967), and Klimenko (1981).

According to Berenson's model, the surface is assumed to be covered by a contiguous vapor film (see Fig. 15). Standing Taylor waves with square λ_d pitch are assumed to develop, and the vapor generated in a square unit cell with λ_d^2 area is assumed to flow toward each vapor dome. For simplicity of modeling, however, the square unit cell is replaced with a circle with radius $r_2 = \lambda_d/\sqrt{\pi}$. The vapor flow is assumed to be laminar, the thickness of the vapor disk is assumed to be constant, and inertia and kinetic energy of the vapor are neglected. The wall heat flux is assumed to be uniform. For the vapor domes, it is also assumed that (see Fig. 15).

Fig. 15 Film boiling on a horizontal surface and schematic of Berenson's model



$$R_B = 2.35\sqrt{\sigma/(g\Delta\rho)}, \quad (34)$$

$$\ell = 1.36 R_B = 3.2\sqrt{\sigma/(g\Delta\rho)}, \quad (35)$$

where $\Delta\rho = \rho_f - \rho_g$. Berenson's analysis continues by solving the momentum equation for the vapor phase and equating the pressure drop in the vapor film with the hydrostatic and surface tension forces associate with the vapor dome. Furthermore, the heat transfer from the wall is assumed to be conducted through the vapor film where a linear temperature distribution is assumed. The analysis, whose details can be found in textbooks (see, e.g., Carey (2008) or Ghiaasiaan (2008)) leads to

$$\delta = \left[1.09C \frac{\mu_v k_v \Delta T}{\rho_v g \Delta \rho h'_{fg}} \sqrt{\sigma/(g\Delta\rho)} \right]^{0.25}. \quad (36)$$

where $C = 12$ if the vapor velocity at the vapor–liquid interphase is assumed to be zero (i.e., no-slip condition), $C = 3$ if zero shear stress at the interphase is assumed, and the corrected latent heat of vaporization, h'_{fg} , is found from Eq. 26 with $C_1 = 0.5$. The heat transfer coefficient can now be found from $\bar{h}_{FB} = k_v/\delta$. The result, after the adjustment of the constant to match experimental data, is

$$\bar{h}_{FB} = 0.425 \left[\frac{k_v^3 \rho_v \Delta \rho g h'_{fg}}{\mu_v (T_w - T_{sat}) \sqrt{\sigma/(g\Delta\rho)}} \right]^{0.25} \quad (37)$$

Properties with subscript v should be calculated at the mean vapor film temperature.

The model of Berenson (1961) as well as Hamil and Baumeister (1967) assumes that the vapor film that separates the vapor domes remains laminar everywhere. Furthermore, they do not apply to small horizontal surfaces (i.e., surfaces that are too small to support a finite number of wavelengths) for which the heat flux is typically larger than the heat flux on large but otherwise similar heated surfaces. Klimenko (1981) developed a model that is similar to the model of Berenson in assuming that vapor domes are formed on a grid that is determined by Taylor instability, but accounts for the occurrence of turbulent flow in the vapor film. Accordingly to Klimenko, the vapor film remains laminar when

$$Ga \left(\frac{\rho_L - \rho_v}{\rho_v} \right) < 10^8 \quad (38)$$

where the Galileo number Ga is defined as

$$Ga = \frac{1}{2} g \lambda_{cr}^2 \quad (39)$$

where $\lambda_{cr} = 2\pi\sqrt{\frac{\sigma}{g\Delta\rho}}$ is the critical (neutral) wavelength associated with two-dimensional Taylor instability. For laminar vapor film, Klimenko (1981) proposed

$$\overline{Nu}_{\lambda_{cr}} = \frac{\overline{h}_{FB}\lambda_{cr}}{k_v} = 0.19 \left[Ga \left(\frac{\rho_L - \rho_v}{\rho_v} \right) \right]^{1/3} Pr_v^{1/3} f_1(Sp) \quad (40)$$

$$f_1(Sp) = \begin{cases} 1 & \text{for } Sp^{-1} \leq 1.4 \\ 0.89Sp^{-1/3} & Sp^{-1} > 1.4 \end{cases} \quad (41)$$

For turbulent vapor film (i.e., when Eq. 38 is not satisfied), Klimenko proposes

$$\overline{Nu}_{\lambda_{cr}} = 0.0086 \left[Ga \left(\frac{\rho_L - \rho_v}{\rho_v} \right) \right]^{1/2} Pr_v^{1/3} f_2(Sp) \quad (42)$$

$$f_2(Sp) = \begin{cases} 1 & \text{for } Sp^{-1} \leq 2.0 \\ 0.71Sp^{-1/2} & Sp^{-1} > 2.0 \end{cases} \quad (43)$$

All vapor properties are to be calculated at mean (film) vapor temperature, i.e., at $(T_w + T_{sat})/2$. The databases for the development of the above correlations included N_2 , H_2 , He, ethane, Freon, pentane, and water, and its recommended range of validity is

$$7 \times 10^4 < Ga \left(\frac{\rho_L - \rho_v}{\rho_v} \right) < 3 \times 10^8; \quad 0.69 < Pr_v < 3.45 \\ 0.031 < Sp^{-1} < 7.3; \quad 0.0045 < P/P_{cr} < 0.98$$

The database includes body force accelerations in the range of g to 21.7 g , where g is the standard terrestrial gravitational acceleration.

The above correlations, as mentioned earlier, underpredict the boiling heat transfer from small surfaces where the development of interfacial waves is not possible. Klimenko (1981) has proposed the following correction to account for the small size of a heated surface:

$$\frac{\overline{Nu}_{\lambda_{cr}}}{\overline{Nu}_{\lambda_{cr}}|_{L/\lambda_{cr} \gg 1}} = \begin{cases} 1 & \text{for } (L/\lambda_{cr}) \geq 5 \\ 2.90(\lambda_{cr}/L)^{0.67} & \text{for } (L/\lambda_{cr}) \leq 5 \end{cases} \quad (44)$$

where L represents the smallest dimension of the horizontal heated surface.

2.4.3 Film Boiling on Cylinders and Spheres

Cylinders. Boiling on the outside surface of a horizontal cylinder is important in view of its occurrence in boilers, heat exchanges, and cryogenic systems.

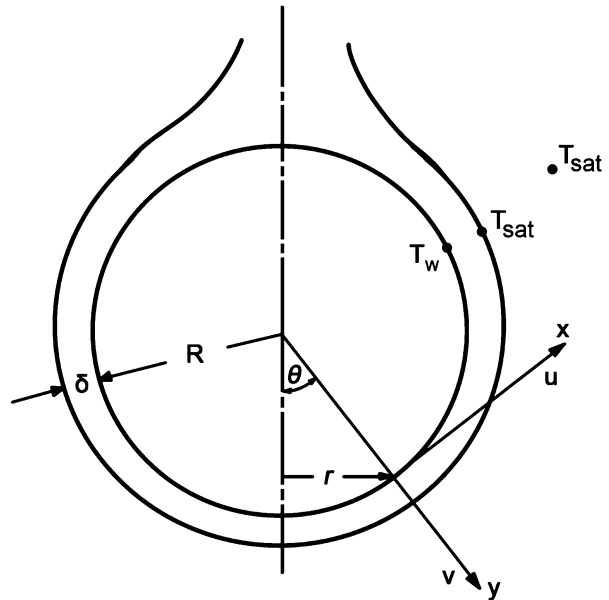
Figure 16 depicts the ideal vapor film flow over a heated cylinder, where the liquid is stagnant, the flow is laminar, and the vapor–liquid interface is smooth. The integral technique can be applied to derive a solution for the vapor film thickness and from there for the local heat transfer coefficient over the circumference of the cylinder. Bromley (1950) derived a solution using the integral method for film boiling in saturated liquid, for the case where the vapor film remains laminar and smooth, the vapor film thickness is everywhere much smaller than the cylinder radius, and assuming that the vapor is incompressible and properties are all constant. Bromley’s solution leads to

$$\bar{h}_{FB} = C \left[\frac{k_v^3 g \rho_v (\rho_L - \rho_v) h'_{fg}}{\mu_v (T_w - T_{sat}) D} \right]^{1/4} \tag{45}$$

The constant C depends on the boundary condition at the vapor–liquid interface: $C = 0.512$ for the static interphase and $C = 0.724$ for the dynamic interphase (see Fig. 13d for the definition of static and dynamic interphase conditions). Bromley chose $C = 0.62$ as an average approximation of the two limits.

Breen and Westwater (1962) compared the predictions of Bromley’s solution with experimental data and noted that Bromley’s correlation is accurate for tube diameters in the range $0.8 < \lambda_{cr}/D < 8$ only. The basic assumptions underlying Bromley’s analysis are violated for very small and very large diameter cylinders. For very small cylinders, the assumption of $\delta/D \ll 1$ may become inapplicable, and therefore some boundary layer approximations may become invalid. Furthermore, for very

Fig. 16 Vapor film during film boiling on a horizontal heated cylinder, when the vapor flow is laminar and smooth



small cylinders, bubbles that engulf the entire circumference of the wire are formed and periodically released on axial intervals that are determined by Rayleigh–Taylor instability. For very large cylinders, interfacial waves (Rayleigh–Taylor in the upper portions and Kelvin–Helmholtz over the lower portions of the circumference) can develop. Accordingly, Breen and Westwater modified Bromley’s correlation according to

$$\bar{h}_{FB} = (0.59 + 0.069C) \left[\frac{g\Delta\rho\rho_v k_v^3 h'_{fg}}{\lambda_{cr}\mu_v(T_w - T_{sat})} \right]^{1/4} \quad (46)$$

where h'_{fg} is found from Eq. 26 with $C_1 = 0.34$, and

$$C = \min(1, \lambda_{cr}/D) \quad (47)$$

Baumeister and Hamil (1967) modeled film boiling on a horizontal cylinder submerged in saturated liquid by analyzing a quasi-steady process over a unit cell consisting of a vapor film that ends in a vapor dome, which is assumed to represent in a time-averaged manner the hydrodynamic instability-driven repetitive pattern of vapor bubble formation and release. Rather than using interfacial wavelengths to define the size of a unit cell, Baumeister and Hamil assumed that the cell size adjusts itself to maximize the rate of heat transfer. They simplified the outcome of their model as

$$\bar{h}_{FB} = 0.373 \left[\frac{g\Delta\rho\rho_v k_v^3 h'_{fg}}{\lambda_{cr}\mu_v(T_w - T_{sat})} \right]^{1/4} \left[1 + \frac{9}{\sqrt{6}} \frac{\lambda_{cr}}{D} + \frac{8}{3\sqrt{6}} \left(\frac{\lambda_{cr}}{D} \right)^3 \right]^{1/4} \quad (48)$$

The analysis that leads to this correlation is valid for $\frac{\lambda_{cr}}{D} > 0.35$, and its validation database included water, helium, oxygen, pentane, ethanol, benzene, Freon 113, isopropanol, and carbon tetrachloride.

Based on experimental data representing several fluids including water, liquid nitrogen, and liquid argon, Sakurai et al. (1990a, b) have developed a semiempirical method (Eq. 50 of Sakurai et al. (1990b) along with Eqs. 71 and 72 of Sakurai et al. (1990a)) for the prediction of film boiling heat transfer coefficient on horizontal cylinders, which can be applied to saturated or subcooled liquid conditions.

Spheres. Boiling on the outer surface of spherical particles is encountered in quenching of such particles during material processing and during fuel-coolant interaction following hypothetical severe accidents in light-water nuclear reactors when core melt occurs and molten nuclear fuel finds its way into the water in the lower plenum. The boiling process starts with film boiling, and film boiling persists, and direct contact between the coolant and the sphere surface is established only when minimum film boiling point is reached.

When natural convection pool boiling occurs on a sphere (i.e., there is no forced flow), and assuming that the vapor film remains laminar, coherent, and smooth, an approximate integral analysis can be performed (Farahat and Nasr 1978; Dhir and Purohit 1978; Hendricks and Baumeister 1969; Tso et al. 1990; Collier and Thome

1994). Referring to Fig. 16, which applies to film boiling on a horizontal cylinder as well as an axisymmetric film boiling on a sphere, assuming that velocity and temperature profiles in the vapor film are both second-order parabolas, and assuming a stagnant interphase (see Fig. 13d), the integral analysis leads to (Farahat and Nasr 1978; Tso et al. 1990)

$$\delta(\theta) = \left[\frac{C_3 \mu_v k_v (T_w - T_{\text{sat}}) D}{g(\rho_f - \rho_v) \rho_v h'_{\text{fg}}} \right]^{1/4} I(\theta) \quad (49)$$

where

$$I(\theta) = \left[\int_0^\theta (\sin \theta')^{5/3} d\theta' \right]^{1/4} / (\sin \theta)^{7/3} \quad (50)$$

The circumferentially averaged film boiling heat transfer coefficient can then be found from

$$\bar{h}_{\text{FB}} = \frac{1}{\pi} \int_0^\pi \frac{k}{\delta(\theta)} d\theta$$

The result is

$$\bar{Nu}_D = \frac{\bar{h}_{\text{FB}} D}{k_v} = C_4 \left[\frac{g(\rho_f - \rho_v) \rho_v D^3}{\mu_v^2} \right]^{1/4} \left[\frac{\text{Pr} h'_{\text{fg}}}{C_{Pv} (T_w - T_{\text{sat}})} \right]^{1/4} \quad (51)$$

The coefficients C_3 and C_4 depend on the assumed temperature and velocity profiles in the vapor film. One finds that $C_3 = 2$ and $C_4 = 0.828$ when the velocity and temperature profiles are

$$\frac{T - T_{\text{sat}}}{T_w - T_{\text{sat}}} = \left[1 - \left(\frac{y}{\delta} \right) \right]^2 \quad (52)$$

$$u = \frac{g(\rho_f - \rho_v) \delta^2 \sin \theta}{2\mu_v} \left(\frac{y}{\delta} \right) \left[1 - \left(\frac{y}{\delta} \right) \right] \quad (53)$$

Note that Eq. 53 is consistent with the stagnant vapor–liquid interphase (see Fig. 13d). Tso et al. (1990) compared Eq. 51 with selected data representing Freon 11, Freon 12, and liquid nitrogen and noted that the equation could bracket the data with $C_4 = 0.696 \sim 1.7$. The above analysis assumes that the vapor film extends over the entire sphere surface and disregards the effect of a vapor bulge that periodically forms over the sphere and leads to periodic release of bubbles.

Frederking and Clark (1963) analyzed laminar film boiling on a sphere and derived an expression similar to Eq. 51 with $C_4 = 0.586$, but noted that to get the best agreement with experimental data, the coefficient C_4 had to be reduced significantly, leading to

$$\overline{Nu}_{D,FB} = 0.14 \left[\frac{g\rho_v(\rho_f - \rho_v)h'_{fg}D^3}{\mu_vk_v(T_w - T_{sat})} \right]^{1/3} \quad (54)$$

The correlations discussed thus far apply to saturation boiling. The enhancement of heat flux caused by liquid subcooling can be significant, however, and must be included. One approximate approach is to simply add together the contributions of saturated film boiling and convection to derive the total heat transfer to subcooled liquid. Dhir and Purohit (1978) proposed

$$\overline{Nu}_{D,FB} = \overline{Nu}_{D,FB,sat} + \overline{Nu}_{D,co} + \overline{Nu}_{D,ra} \quad (55)$$

where, as noted, the contributions of film boiling, convection, and radiation are simply added together. The heat transfer coefficient representing the sum of these contributions and the wall heat flux are found, respectively, from the following two expressions:

$$q''_w = \overline{h}_{FB}(T_w - T_{sat}) \quad (56)$$

$$\overline{Nu}_{D,FB} = \overline{h}_{FB}D/k_v = \frac{q''_w D}{k_v(T_w - T_{sat})} \quad (57)$$

where

$$\overline{Nu}_{D,FB,sat} = 0.8 \left[\frac{g\rho_v(\rho_f - \rho_v)h'_{fg}D^3}{\mu_vk_v(T_w - T_{sat})} \right]^{1/4} \quad (58)$$

$$\overline{Nu}_{D,co} = 0.9 \left[\frac{g\rho_L^2 - C_{PL}\beta_L(T_{sat} - T_{L,\infty})D^3}{\mu_L k_L} \right]^{1/4} \quad (59)$$

The last term on the right side of Eq. 55 represents the contribution of radiation heat transfer and will be discussed shortly.

2.5 The Effect of Thermal Radiation in Film Boiling

When convection and radiation take place simultaneously, it is often sufficient to simply add the convective and radiative heat transfer coefficients. This approach will

be correct, however, only when two conditions are met. First, the temperature of the surroundings (with which radiative heat exchange takes place) should be equal to the fluid bulk temperature, and second convective and radiative heat transfer mechanisms must not be coupled. The latter condition is not met in film boiling, because the added cooling effect by radiative heat transfer modifies the vapor film characteristics (i.e., reduces the film thickness and may even affect the film's flow regime), and therefore affects the convective heat transfer that takes place through the vapor film. Radiation and convection heat transfer mechanisms are thus coupled, and simply adding the convective and radiative heat transfer coefficients may not be correct.

Bromley (1950) recommended that for film boiling in a saturated liquid, the total heat transfer coefficient be calculated from

$$h_{\text{tot}} = h_{FB}(h_{FB}/h_{\text{tot}})^{1/3} + h_{\text{rad}} \quad (60)$$

where h_{FB} is the film boiling heat transfer coefficient in the absence of radiation effect, and h_{tot} is the heat transfer coefficient due to the combined contributions of the two mechanisms. Lubin (1969) showed that the above expression can be justified for laminar film boiling on a vertical surface. The radiative heat transfer coefficient can be found from the following expression, which represents radiative heat transfer between two infinitely large diffuse and gray parallel plates, if the vapor is assumed to be transparent to thermal radiation:

$$h_{\text{rad}} = \frac{\sigma_{SB}(T_w^4 - T_{\text{sat}}^4)}{\left(\frac{1}{\varepsilon_w} + \frac{1}{\varepsilon_l} - 1\right)(T_w - T_{\text{sat}})} \quad (61)$$

where ε_w and ε_l represent the total, hemispherical radiative emissivities of the wall and the liquid–vapor interphase, respectively. In most application, however, $\varepsilon_l \approx 1$, which leads to the following simpler expression:

$$h_{\text{rad}} \approx \frac{\sigma_{SB}\varepsilon_w(T_w^4 - T_{\text{sat}}^4)}{T_w - T_{\text{sat}}} \quad (62)$$

Equation 60 requires an iterative solution for the total heat transfer coefficient. The following simpler expression (Bromley et al. 1953) appears to do well in predicting experimental data:

$$h_{\text{tot}} = h_{FB} + \frac{3}{4}h_{\text{rad}}, \quad (63)$$

Sakurai et al. (1990a) have derived an expression for h_{tot} for film boiling on the outside of a horizontal cylinder, based on the numerical solution of the liquid and vapor conservation equations assuming a laminar and smooth vapor film.

2.6 Minimum Film Boiling Heat Flux and Temperature

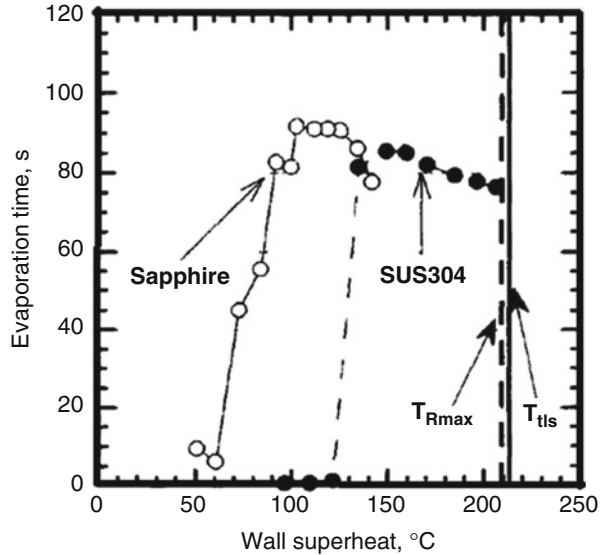
2.6.1 General Remarks

The minimum film boiling (MFB) point, also referred to as minimum heat flux (MHF) point, represents the lowest point in the part of the boiling curve where wall superheat is larger than the wall superheat representing the critical heat flux point and defines the boundary between film and transition boiling regimes. MFB point is an important threshold, particularly for transient boiling processes, e.g., quenching. The conditions that lead to MFB are sensitive to surface conditions and vary over a wide range. Parameters that can affect MFB include surface configuration and dimensions, pressure, liquid subcooling, surface wettability and roughness, thermophysical properties of the heated surface in particular its thermal conductivity, and whether the MFB represents a steady state or transient process. As a result models and correlations for the MFB temperature T_{MFB} or heat flux q''_{MFB} are not very accurate, and a relatively large uncertainty should be expected when such models are applied.

The simplest models for MFB assume that MFB point simply represents the end of the film boiling regime, whereby when $T_w > T_{MFB}$ (or $q''_w > q''_{MFB}$), it is assumed that essentially no macroscopic physical contact between liquid takes place. However, as mentioned earlier, experimental observations have shown that some liquid–surface contact occurs at least in the portion of the boiling curve designated as film–transition boiling in Fig. 5.

A phenomenon closely related to MFB is the Leidenfrost process, first reported in 1756 by the German scientist J.G. Leidenfrost. It refers to the dancing motion of a liquid droplet on a very hot surface, which takes place because of the formation of a vapor cushion that is typically of the order of 10 μm thick (Biance et al. 2003) between the droplet and the hot surface. If the surface temperature is gradually reduced, eventually *Leidenfrost point* (LP) is reached, when the surface temperature reaches the *Leidenfrost temperature*, at which point the heat transfer rate between the droplet and the surface is at its minimum. With further lowering of the temperature of the surface, more extensive contact between the droplet and surface takes place, and stable film boiling is terminated. A practical experimental method for determining the LP is by measuring the lifetime of droplets of a particular liquid with identical initial conditions as a function of the heated surface temperature. Figure 17, as an example, shows the evaporation curve for saturated water droplets with initial diameters of 3.5 mm dropped on hot sapphire and stainless steel surfaces (Nagi and Nishio 1996). Figure 18 shows qualitatively the boiling regimes and their dependence on wall superheat that occur during the Leidenfrost process. Each evaporation curve represents the variation of droplet lifetime as a function of wall superheat, and the point representing the maximum lifetime represents the LP. For the points on an evaporation curve to the left of the LP, there is partial contact between the liquid and surface which leads to faster evaporation and shorter droplet lifetime. For the points to the right of the LP, on the other hand, there is stable film boiling, and there is essentially no physical contact between the liquid and surface. For wall superheats larger than the wall superheat

Fig. 17 Evaporation curve for water droplets with 3.5 mm initial diameter (after Nagi and Nishio 1996)



at the LP point, however, with increasing the surface temperature, the heat transfer rate increases, and therefore the droplet lifetime becomes shorter. The main difference between LP obtained with small liquid droplets and MFB in pool boiling is that in experiments with sessile droplets, the area underneath the droplet where a vapor film forms is typically too small to allow for the development of interfacial waves, whereas in pool boiling experiments, the surface area is often large enough to allow for the development of liquid–vapor interfacial waves. However, this discrepancy is important if the vapor film hydrodynamic instability, to be discussed shortly, is the mechanism leading to MFB. Furthermore, experiments have shown that the LP point is not sensitive to initial droplet size (Gottfried et al. 1966; Patel and Bell 1966; Nishio 1983).

In terms of the physical processes that lead to MFB, a number of different mechanisms have been proposed and used for model development. The proposed models can generally be divided into two categories:

1. Heat flux-controlled models. Hydrodynamically, controlled vapor film instability models are examples of this group of models (Zuber 1959; Berenson 1961; Lienhard and Wong 1964). According to these models, during stable film boiling, the vapor film–liquid interface supports Taylor waves that grow and lead to the formation and release of bubbles. If the vapor generation rate is reduced to a level that the periodic formation and release of bubbles are no longer sustainable, then the vapor film will collapse at some points. The lowest vapor generation rate (equivalently, the lowest heat flux) that can sustain a coherent and stable vapor film will represent the MFB conditions. The hydrodynamic models are widely used but suffer from a number of shortcomings. Hydrodynamic models that assume the occurrence of a coherent vapor film do not

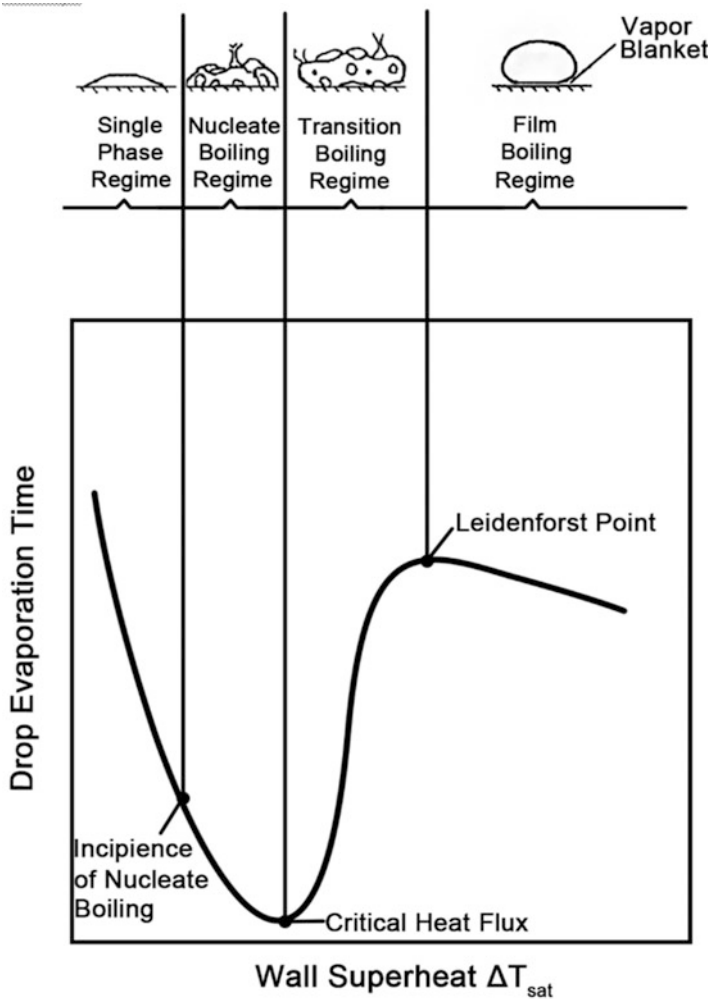


Fig. 18 Sessile droplet evaporation curve and the associated boiling regimes (after Bernardin and Mudawar 1999)

explicitly account for the effect of surface conditions and properties. Experiment has shown that surface wettability and cleanliness have a significant effect on MFB (Chowdury and Winterton 1985, Bui and Dhir 1985a; Bernardin and Mudawar 1999). These models also apply when the surface size is large enough to support interfacial waves and depend on surface configuration. Some experimental data suggest that surface configuration has little effect on MFB, however (Nishio et al. 1987).

2. Temperature-controlled models. In these models, MFB is assumed to occur when the surface temperature, and consequently the temperature of the liquid layer

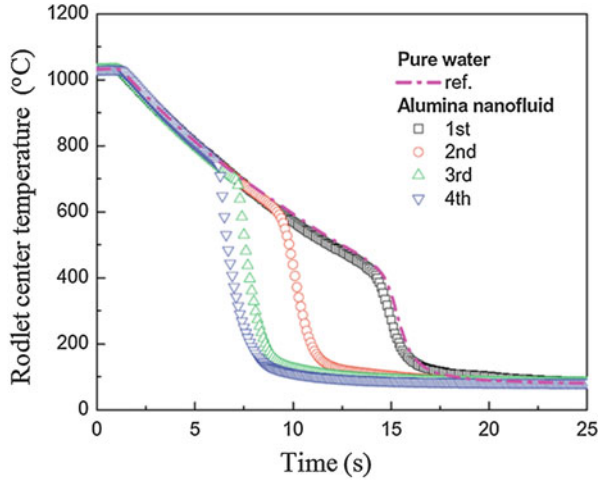
interacting with it, exceeds some threshold. Recall that the liquid in contact with a hot surface becomes superheated during nucleate boiling. The local superheat that is needed for heterogeneous bubble nucleation is typically small. The MFB point, however, typically represents significantly higher wall superheats in comparison with heterogeneous nucleation in pool boiling. (Cryogenic fluids are an exception, however, and MFB happens for them at relatively low wall superheats.) These assumed threshold temperatures include the liquid spinodal temperature or the temperature that can cause homogeneous vapor nucleation.

Mechanisms that have been used as the bases of models for MFB also include the hypothesis that MFB occurs when the temperature of the liquid in contact with surface reaches a level that causes perfect spreading (Olek and Zvirin 1988). Based on the observation that sessile droplets after impacting a hot surface separate from the surface while they are at their maximum spreading, and using an expression for the dependence of contact angle on temperature suggested by Adamson and Ling (1964), Olek et al. suggested that the temperature representing zero contact angle can be used as an upper limit for MFB. Segev and Bankoff (1980) also have proposed a mechanism for MFB based on the adsorption characteristics of the surface. In this hypothesis, a non-evaporating precursor (adsorbed) liquid film must spread on the surface in advance of a thicker liquid film that wets the surface and evaporates. The precursor film thickness decreases as the surface temperature increases, and the MFB occurs at a threshold temperature at which the precursor film thickness goes through a sharp decline. The above mechanisms have not found wide acceptance, however.

The effect of the deposition of nanoparticle films of surfaces and the consequent improvement in CHF and nucleate boiling heat flux were already mentioned in Sect. 2.3. Deposited nanoparticles appear to increase the minimum film boiling temperature and minimum heat flux. Kim et al. (2010) performed quenching experiments with metallic spheres and cylindrical rodlets in 0.1% volume aqueous nanofluids (water containing 0.1% volume nanoparticles) under atmospheric pressure conditions. The rodlets were vertically plunged in the coolant liquid pool. The deposition of nanoparticles increased MFB (quenching) temperature and heat flux, as well as the quench front speed. Figure 19 depicts their quenching results with a 4.8-mm-diameter rodlet cooled in subcooled alumina nanofluid. The depicted data show the experimental measurements with the rodlet in pure water and in four repetitions of the experiment, this time with the nanofluid. As noted, in the first pass (the first test with nanofluid), the temperature profile is identical to pure water. In the subsequent passes, however, the temperature profiles show that CHF and MFB heat flux are both enhanced as a result of the deposition of nanoparticles on the surface. The improvement diminishes after the third pass, however, apparently due to the diminishing rate of particle deposition.

Experimental data also suggest that the effect of liquid velocity on MFB conditions is insignificant (Sakurai 1984; Nishio 1987).

Fig. 19 Center temperature histories during quenching of 4.8-mm-diameter metallic rodlets quenched by vertically plunging in pure water and aqueous 0.1% volume alumina nanofluid (Kim et al. 2010). The water subcooling was 20 °C



2.6.2 Predictive Methods for MFB

Correlations for MFB that represent temperature-controlled MFB phenomenology include a reduced-state Leidenfrost temperature correlation by Baumeister and Simon (1973):

$$T_{MFB} = \frac{27}{32} T_{cr} \left\{ 1 - \exp \left[-0.52 \left(\frac{10^4 (\rho_w / A_w)^{4/3}}{\sigma} \right)^{1/3} \right] \right\} \tag{64}$$

where A_w and ρ_w are the atomic number and density (in grams per cubic centimeter) of the heated surface, T_{MFB} and T_{cr} are the MFB and the critical temperature of the fluid in absolute scale, and σ is the liquid–vapor surface tension (in dynes per centimeter). The correlation evidently depends on the fluid–solid pair properties and has been tested against some refrigerant, cryogenic, and high surface tension fluids such as mercury. This correlation also agreed quite well with the experimental data of Bernardin and Mudawar (1999) representing Leidenfrost phenomenon of acetone, benzene, F-72, and water on aluminum surfaces with polished, particle-blasted, and rough-sanded surfaces.

Kalinin et al. (1969) have proposed the following correlation which accounts for the effect of the solid surface thermophysical properties, as well as the subcooling of the liquid, and has been found to agree well with cryogenic fluid experiments for pool as well as forced flow boiling (Pron’ko and Bulanova 1978):

$$\frac{T_{MFB} - T_{sat}}{T_{cr} - T_L} = 0.165 + 2.5 \left[\frac{(\rho Ck)_f}{(\rho Ck)_w} \right]^{0.25} + \frac{(\rho Ck)_f}{(\rho Ck)_w} \tag{65}$$

The correlation is suitable for well-wetting surface–liquid pairs, and its range of validity, when applied to internal flow, is (Groeneveld and Snoek 1986)

$$10^{-3} < \frac{(\rho Ck)_f}{(\rho Ck)_w} < 1; \frac{T_{\text{sat}} - T_L}{T_{\text{cr}} - T_{\text{sat}}} \leq 1.5; 0.02 \leq P/P_{\text{cr}} \leq 0.68$$

$$D_H \geq 10 \sqrt{\frac{\sigma}{g(\rho_L - \rho_g)}}, \text{Re}_{D_H, L} \leq 1.4 \times 10^5; U_{L, m} \left(\frac{\sigma g}{\rho_L - \rho_g} \right)^{-1/4} \leq 160$$

Based on a careful review of experimental data, Nishio (1987) concluded that surface wettability and pressure were important parameters that affect MFB temperature. However, noting that for common fluids boiling on commonly applied clean metallic surfaces the contact angle varies in a relatively narrow range, Nishio proposed the following correlation:

$$T_{\text{MFB}} = T_{\text{sat}} + 3.449$$

$$\times 10^{-4} \left(\frac{T_{\text{cr}} - T_{\text{sat}}}{T_{\text{cr}} - T_{\text{sat}}^*} \right) \left(\frac{h_{fg}^*}{C_{pf}^*} \right) (\rho_r^*)^{0.6302} (\text{Pr}_f^*)^{1.008} (L_r^*)^{0.2056}$$

$$\cdot \exp[4.94(T_{\text{sat}}/T_{\text{cr}})] \quad (66)$$

where $\rho_r = \rho_g/\rho_f$ and L_r is a dimensionless number defined as

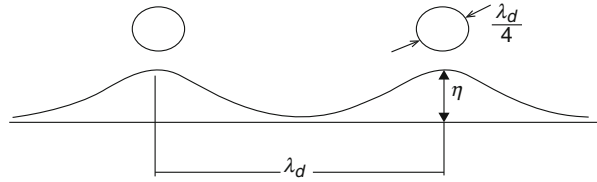
$$L_r = \frac{\sigma^3}{g(\rho_f - \rho_g)^3 \nu_f^4}$$

All quantities with * superscript in this expression are to be calculated at a reference temperature defined as $T_{\text{ref}} = 0.7T_{\text{cr}}$.

Models based on hydrodynamic-controlled MFB hypothesis will now be reviewed. These widely used models, as mentioned earlier, are based on the hypothesis that MFB is a heat flux-controlled process. They are most successful for liquid–solid pairs with good wetting and are therefore often suitable for commonly applied liquids boiling on clean metallic surfaces.

Zuber (1959) developed a model for MFB on a horizontal surface by assuming that the process is driven by Taylor instability, as depicted in Fig. 20. According to this model, bubbles are formed on a two-dimensional grid with a pitch that should be in the $\lambda_{\text{cr}} < \lambda < \lambda_d$ range. Assuming a spacing of $\lambda_d = 2\pi\sqrt{3}\sqrt{\sigma/g\Delta\rho}$, in each cycle, a bubble grows and is released at every grid point (see Fig. 20). The bubbles grow as a result of the growth of Taylor waves, and the growth rate of the Taylor wave nodes corresponds to the fastest-growing wavelength predicted by Taylor

Fig. 20 Hydrodynamics of MFB according to the model of Zuber (1959)



instability. It is also assumed that bubble release takes place when the peak rises to a height of $\lambda_d/2$, but the released bubble is a sphere with a radius of $\lambda_d/4$. The details of the derivation can be found in textbooks (e.g., Ghiaasiaan 2008). Zuber's analysis thus leads to the following expression when $\rho_v \ll \rho_f$:

$$q''_{\text{MFB}} = C_1 \rho_v h_{\text{fg}} \left[\frac{\sigma g \Delta \rho}{(\rho_f + \rho_g)^2} \right]^{1/4} \quad (67)$$

Zuber's analysis leads to $C_1 = 0.176$. This expression with the latter value for C_1 was found to overpredict experimental data, however. Based on experimental data, Berenson (1961) modified the coefficient to $C_1 = 0.091$ and replaced h_{fg} with h'_{fg} to account for the effect of vapor film superheating. Knowing q''_{MFB} and h_{MFB} (the latter from Eq. 37), the surface temperature at MFB, namely, T_{MFB} , can be calculated from

$$(T_{\text{MFB}} - T_{\text{sat}})_{\text{Berenson}} = (q''_{\text{MFB}}/h_{\text{FB}})_{\text{Berenson}} \quad (68)$$

The above analysis, as noted, assumes that stable film boiling applies all the way to the MFB point. Furthermore, it does not account for any effect of surface properties. However, experimental data show that the thermophysical properties of the heated surface affect T_{MFB} (Moreaux et al. 1975; Zhukov et al. 1975; Yao and Henry 1978). As explained earlier, when the MFB is approached from the film boiling side of the boiling curve, the boiling curve deviates from the pure film boiling line at a temperature higher than MFB temperature (film–transition boiling region; see Fig. 5), and this deviation is caused by sporadic liquid–wall contact that takes place near the nodes of the waves that form at the vapor–liquid interphase in film boiling. The surface temperature is thus affected by heat conduction in the solid phase. An analysis that corrects Berenson's model for the effects of the solid surface thermophysical properties was developed by Henry (1974). Based on data representing boiling of liquid sodium and potassium on tantalum (*Ta*) and stainless steel, respectively, water and refrigerant Freon 11 on stainless steel, Freon 11 on Teflon, and ethanol on glass, Henry proposed

$$\frac{T_{\text{MFB}} - T_{\text{MFB, Berenson}}}{T_{\text{MFB, Berenson}} - T_L} = 0.42 \left[\sqrt{\frac{(\rho Ck)_f}{(\rho Ck)_w}} \frac{h_{\text{fg}}}{C_w (T_{\text{MFB, Berenson}} - T_{\text{sat}})} \right]^{0.6} \quad (69)$$

This form of the correction factor can be better understood by noting that when a liquid particle contacts the hot surface, during the ensuing short transient, the thermal interaction at the surface is similar to heat conduction between two initially isothermal semi-infinite media that abruptly come into contact. The interface temperature between the two stagnant semi-infinite media, one representing the wall and the other representing the liquid, will then be governed by

$$T_I = \frac{(\rho_L C_{PL} k_L)^{1/2} T_{L, \infty} + (\rho_w C_w k_w)^{1/2} T_{w, \infty}}{(\rho_L C_{PL} k_L)^{1/2} + (\rho_w C_w k_w)^{1/2}} \quad (70)$$

where $T_{w, \infty}$ is the temperature in the wall material far away from the wall–fluid interface, and $T_{L, \infty}$ is the liquid bulk temperature. It can be easily noted that the correction on the film boiling temperature predicted by the correlation of Henry (1974) is small when the surface is highly conductive (more precisely, when $\frac{(\rho Ck)_f}{(\rho Ck)_w} \ll 1$), in which case the solid–liquid interface temperature remains close to the bulk solid temperature during short liquid–surface contacts. For a surface material that has a low thermal conductivity (i.e., when $\frac{(\rho Ck)_f}{(\rho Ck)_w}$ is not very small), however, the correction will be significant.

2.7 Transition Boiling

In transition boiling as mentioned earlier, the heated surface is partially in nucleate boiling and partially in film boiling. The phenomenological aspects of transition boiling, as well as the important issue of hysteresis, were discussed in sections “[Boiling Curve Hysteresis](#)” and “[Parametric Effects](#).” Predictive methods will be discussed in this section.

The transition boiling regime is poorly understood and has received relatively little research attention in the past. Industrial systems usually are not designed to operate in this regime. However, transition boiling is important in transient processes, particularly during the quenching of hot surfaces. Quenching of hot surfaces occurs during the reflood phase of a loss of coolant accident (LOCA), when the hot and partially dry fuel rods are subjected to water supplied by the reactor’s emergency cooling system. Quenching is also a widely used technique in material processing and can occur under accident conditions in superconductors, as well as during the chill-down of cryogenic liquid transfer lines.

Some important parametric trends in transition boiling are the following:

- (a) Surface roughness moves the transition boiling line in the boiling curve toward the left, thus deteriorating the transition boiling heat transfer coefficient (see Fig. 10).
- (b) Improved wettability (lowering of contact angle) improves (increases) the transition boiling heat transfer coefficient.
- (c) In transient tests, the transition boiling line obtained with transient heating (increasing T_w) is higher than with transient cooling (decreasing T_w).

Dhir and Liaw (1989) have proposed a framework for a unified mechanistic modeling of nucleate and transition boiling, which should apply to fully developed nucleate boiling as well as transition boiling. In the fully developed nucleate boiling regime (see Fig. 2), evaporation appears to occur primarily at the periphery of the vapor stems in the liquid macrolayer, which refers to the liquid film that separates the heated surface from the base of the vapor mushroom. Dhir and Liaw (1989) argued that in TB, fully developed nucleate boiling takes place over the part of the surface that is in contact with liquid and film boiling occurs on the remainder of the surface; therefore, one can write

$$\begin{aligned} \bar{q}''_{TB}(T_w) &= (1 - \bar{\alpha}_w)\bar{q}''_L + \bar{\alpha}_w\bar{q}''_v \\ &= (1 - \bar{\alpha}_w)\bar{h}_{NB}(\bar{T}_w - T_{sat}) + \bar{\alpha}_w\bar{h}_{FB}(\bar{T}_w - T_{sat}) \end{aligned} \quad (71)$$

where all quantities with bars are time-averaged. (All those parameters fluctuate with time during transition boiling. The locations where either of the two boiling regime occurs also move from point to point on the surface.) Furthermore, $\bar{\alpha}_w$ is the time-averaged void fraction adjacent to the wall, and \bar{h}_{NB} represents the heat transfer coefficient for fully developed nucleate boiling. Dhir and Liaw obtained \bar{h}_{NB} by modeling the heat transfer in the macrolayer and the evaporation process over the circumference of the vapor stems, where the contact angle affects the geometry of the vapor stems. To apply this model, one would need to know the time-averaged void fraction next to the wall, $\bar{\alpha}_w$, however.

Most of the widely used correlations for transition boiling are empirical, do not consider hysteresis, and are based on interpolations either between CHF and MFB points or between nucleate boiling and film boiling heat transfer rates based on local conditions. These correlations are often in one of the following forms:

$$q''_{TB}(T_w) = Fq''_{CHF} + (1 - F)q''_{MFB} \quad (72)$$

$$\begin{aligned} \bar{q}''_{TB}(T_w) &= F\bar{q}''_{NB} + (1 - F)\bar{q}''_{FB} \\ &= F\bar{h}_{NB}(\bar{T}_w - T_{sat}) + (1 - F)\bar{h}_{FB}(\bar{T}_w - T_{sat}) \end{aligned} \quad (73)$$

where F represents the time-averaged fraction of the total heated surface that is in contact with liquid. Equation 72 satisfies the important and obvious requirement that the total heat flux should approach the critical heat flux at the limit of $F = 1$,

and it should approach the minimum heat flux at the limit of $F = 0.0$. It also ensures that the heat flux on the wetted portions of the surface does not exceed critical heat flux on one hand and does not fall below MFB heat flux on the other. Equation 72 has been used in some of the widely applied correlations in the past; however, it has the disadvantage that there is much uncertainty in the predictive models and correlations for q''_{CHF} and in particular for q''_{MFB} . In Eq. 74, \bar{q}''_{NB} and \bar{h}_{NB} represent nucleate boiling heat flux and heat transfer coefficient, respectively, which occur over the parts of the heated surface that are in contact with liquid coolant. These parameters are in general not well understood, however, and their dependence on local parameters including F is unclear. Likewise, \bar{q}''_{FB} and \bar{h}_{NB} are the time-averaged heat flux and heat transfer coefficient, respectively, which occur over the dry portions of the heated surface.

A correlation proposed by Bjonard and Griffith (1977) is based on Eq. 72 where

$$F = \left(\frac{T_{MFB} - T_w}{T_{MFB} - T_{CHF}} \right)^2 \quad (74)$$

A linear interpolation on a log–log scale is recommended by Haramura (1999):

$$\frac{\ln[q''_{TB}(T_w)/q''_{MFB}]}{\ln(q''_{CHF}/q''_{MFB})} = \frac{\ln[(T_{MFB} - T_{sat})/(T_w - T_{sat})]}{\ln[(T_{MFB} - T_{sat})/(T_{w,CHF} - T_{sat})]} \quad (75)$$

3 Flow Boiling

Distinction should be made between *external flow* and *internal flow boiling*. In external flow boiling, the heated surface is typically surrounded by a large liquid field, and the processes that take place at the vicinity of the heated surface have little effect on the far-field flow. Furthermore, the surrounding coolant is either subcooled or saturated liquid or a low-quality liquid–vapor mixture. The quenching of metallic balls is a good example, where droplets of liquid metal are released into a standing body of liquid coolant, and the flow is caused by the gravity-induced motion of the metal droplet. In internal flow boiling, on the other hand, the flow takes place in a confined space, and the properties of the bulk flow change as a result of evaporation. The forthcoming discussions will be focused on internal flow boiling.

Internal flow boiling is considerably more complicated than pool boiling because of the coupling between hydrodynamics and heat transfer processes. A sequence of two-phase and boiling heat transfer regimes takes place along the heated channel during flow boiling, as a result of the increasing flow quality. The two-phase flow regimes in a boiling channel are therefore “developing” everywhere and are morphologically different than their namesakes in adiabatic two-phase flows.

3.1 Forced-Flow Boiling Regimes

The preferred configuration for boiling channels is vertical and upflow. In this configuration, buoyancy helps the mixture flow. However, flow boiling in horizontal and even vertical channels with downflow is also of interest. Horizontal boiling channels are not uncommon, and flow boiling in a vertical, downward configuration may occur under accident conditions in systems that have otherwise been designed to operate in liquid single-phase forced convection heat transfer conditions.

The heat transfer regimes of interest in this section, namely, transition and film boiling, occur downstream from the critical heat flux (CHF) point. These regimes depend on the CHF type. (For detailed discussion of flow boiling phenomena, including CHF and related topics, see Ghiaasiaan (2017).) Figure 21 displays schematically the heat transfer, two-phase flow, and boiling regimes that take place in a vertical tube with upward flow (which is the preferred configuration for boiler channels) that operates in a steady state and is subject to a uniform and moderate heat flux. The mass flow rate is assumed constant. In the displayed channel, *dryout*-type CHF takes place. The dryout point is preceded by forced convective evaporation where the flow regime is annular or annular dispersed. This is an extremely efficient heat transfer regime. Droplet entrainment can occur when vapor flow rate is sufficiently high. The vapor quality and therefore the void fraction are quite high downstream the dryout point (void fraction is 90% or higher), and the heat transfer regime is *dispersed droplet film boiling*. Transition boiling is thus absent.

Fig. 21 Two-phase flow and boiling regimes in a vertical pipe with a moderate wall heat flux

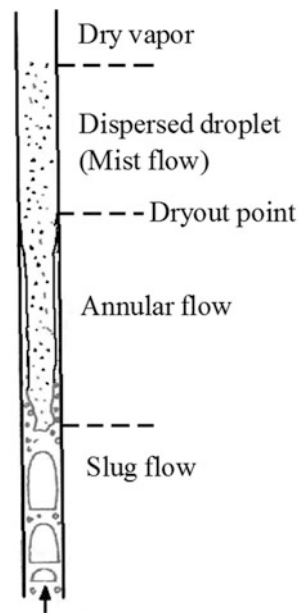


Fig. 22 Two-phase flow and boiling regimes in a vertical pipe with a high wall heat flux

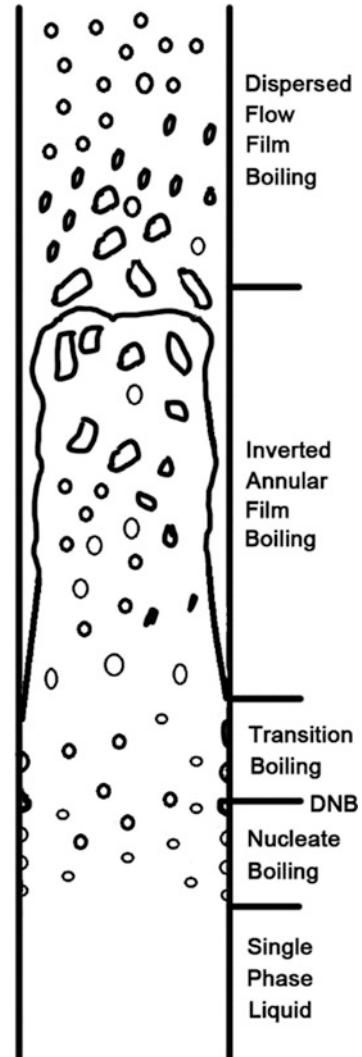


Figure 22 displays the flow and heat transfer regimes in a vertical heated channel subject to a high heat flux. The flow patterns are different than those in Fig. 21. Because of the high wall heat flux, onset of nucleate boiling (ONB) takes place in the channel, while the bulk liquid is subcooled. Nucleate boiling takes place downstream from the ONB point, a growing bubbly layer may form adjacent to the wall, and the bubbles may eventually disrupt macroscopic contact between the liquid and heated surface. This leads to the *departure from nucleate boiling* (DNB). The heat transfer coefficient, which is very high in the subcooled boiling regime, deteriorates very significantly downstream from the DNB point, even

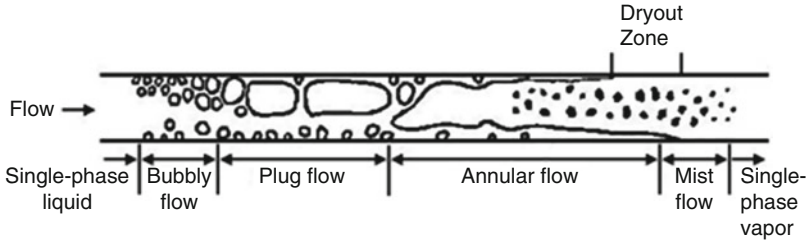


Fig. 23 Flow and heat transfer regimes in a uniformly heated horizontal tube with moderate heat flux

though the bulk flow may still be subcooled. In this case, the post-CHF heat transfer regimes include transition boiling, stable film boiling, as well as dispersed droplet film boiling.

Horizontally oriented channels are used in boilers and some nuclear reactor designs. In horizontal flow passages when the coolant flow rate is high, the two-phase flow and the heat transfer regimes are insensitive to the flow passage orientation and are similar to those in a vertical and upward flow passage. With high wall heat flux, DNB occurs in such channels and is followed by transition, stable film, and dispersed droplet film boiling heat transfer regimes. At low flow rates, however, in commonly applied channels (excluding mini- and microchannels), the tendency of the two phases to stratify results in the occurrence of “early” dryout (see Fig. 23). The liquid film tends to drain downward, often leading to *partial dryout*, where the liquid film breaks down near the top of the heated channel, while persisting in the lower parts of the channel perimeter. Downstream the dryout point, the heat transfer regime is dispersed droplet film boiling, which eventually changes into forced convection by vapor once the evaporation of the entrained droplets is complete.

The boiling curve (heat flux vs. wall superheat curve) for internal flow depends on coolant mass flux and the flow quality, in addition to other parameters that affect the pool boiling curve. Figure 24 displays the boiling curve when the mass flux is constant and the flow quality is constant and low, for a vertical and upward pipe flow. This boiling curve can be generated in repeated experiments in which the mass flux and local quality are maintained constant, while the heat flux is varied and the wall superheat is measured.

The effects of mass flux and equilibrium quality on the boiling curve are shown in Fig. 25a, b, respectively. The heat transfer coefficient is particularly sensitive to mass flux in the post-CHF regimes. The effect of local quality on post-CHF regimes is rather complicated. When DNB-type CHF occurs, the post-CHF heat transfer coefficients may decrease with increasing local quality. Following dryout, when the quality is relatively high, however, the mixture velocity increases with increasing quality, and as a result, the local heat flux and heat transfer coefficient may increase as well.

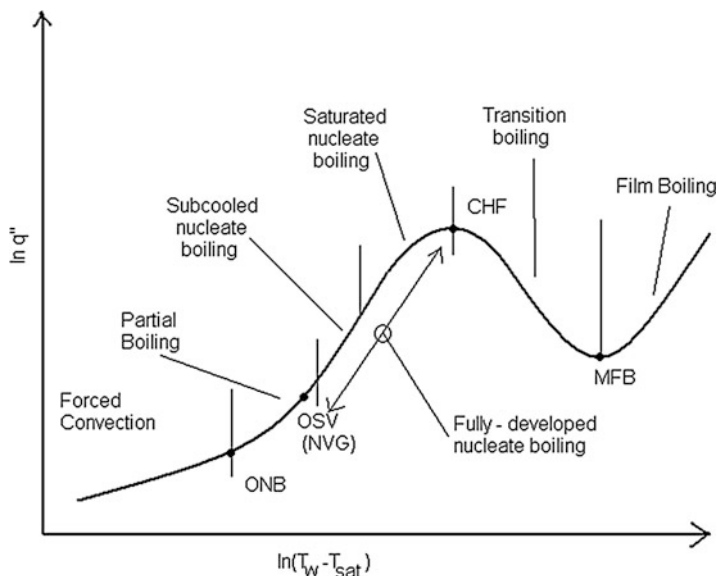


Fig. 24 The flow boiling curve for low qualities

3.2 Minimum Film Boiling Point and Transition Boiling

For MFB, pool boiling correlations are often used (see Sect. 2.6). Purely empirical correlations that are applicable for water and heated surfaces that are common in water-cooled reactor cores are available, however. An example is the correlation of Stewart and Groeneveld (Stewart and Groeneveld 1981; Groeneveld and Stewart 1982; Groeneveld and Snoek 1986), which is suitable for horizontal flow passages with an Inconel-heated surface.

Correlations for flow MFB are often based on quenching data over limited ranges of parameters. Unlike pool boiling, using a simple interpolation between the CHF and the MFB points (although such interpolations are common) is not always straightforward because the conditions at the MFB point are not unique and may not be known a priori. Some examples, all of which are for water, follow.

The correlation of Bjonard and Griffith (1977) (Eqs. 72 and 74) has already been mentioned in Sect. 2.7. This correlation is applied for flow boiling as well.

The correlation of Ramu and Weisman (1974) is

$$h_{TB} = 500S\{\exp[-0.14(\Delta T - \Delta T_{CHF})] + \exp[-0.125(\Delta T - \Delta T_{CHF})]\} \quad (76)$$

where T is in kelvins, h_{TB} is in watts per meter squared per kelvin, S is Chen's suppression factor (Chen 1966) based on local mass flux and quality, and $\Delta T = T_w - T_{sat}$ and $\Delta T_{CHF} = T_{CHF} - T_{sat}$. Chen's suppression factor can be found from (Collier 1981)

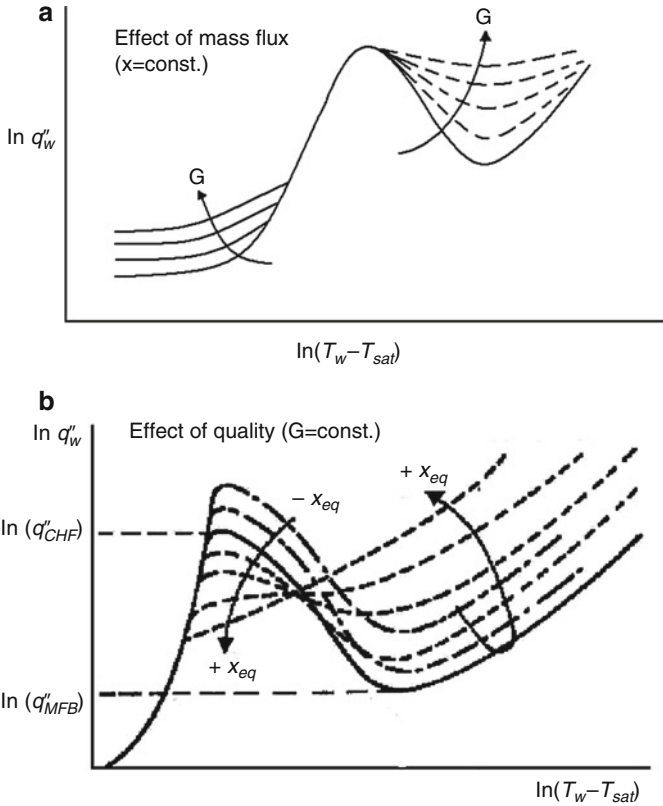


Fig. 25 Effects of local quality and mass flux on the flow boiling curve (After Groeneveld 1986)

$$S = \left[1 + (2.56 \times 10^{-6}) (\text{Re}_f F^{1.25})^{1.17} \right]^{-1} \tag{77}$$

where

$$F = \begin{cases} 1 & \text{for } \frac{1}{X_{tt}} < 0.1, \\ 2.35 \left(0.213 + \frac{1}{X_{tt}} \right)^{0.736} & \text{for } \frac{1}{X_{tt}} > 0.1. \end{cases} \tag{78}$$

$$X_{tt} = \left(\frac{\rho_g}{\rho_f} \right)^{0.5} \left(\frac{\mu_f}{\mu_g} \right)^{0.1} \left(\frac{1 - x_{eq}}{x_{eq}} \right)^{0.9} \tag{79}$$

$$\text{Re}_f = G(1 - x_{eq})D_H/\mu_f \tag{80}$$

The following correlation (Weisman 1981) is based on data with water at pressures in the 1–4 bars pressure and is used for modeling the bottom quenching of rod bundles (bottom reflooding):

$$h_{TB} = h_{CHF} \cdot \exp[-0.04(T_w - T_{w,CHF})] + 4500 \left(\frac{G}{G_{ref}} \right)^{0.2} \cdot \exp[-0.012(T_w - T_{w,CHF})] \quad (81)$$

where SI unit system is used (temperatures are in K and heat transfer coefficients are in $W/m^2.K$), T_w is the local wall temperature, $T_{w,CHF}$ is the wall temperature at the CHF point, and

$$G_{ref} = 67.8 \text{ kg}/m^2.s \quad (82)$$

$$h_{CHF} = q''_{CHF} / (T_{w,CHF} - T_{sat}) \quad (83)$$

The correlation of Weisman (1981) is evidently based (anchored on) the CHF point and does not use the conditions at MFB at all.

Thermal hydraulic codes that have been developed for nuclear reactor safety analysis often utilize purely empirical and multistep procedures for calculating the wall heat flux that lead to good agreement with experimental data (see, e.g., RELAP5-3D Code Development Team (2012)). The RELAP5-3D code, for example, uses the aforementioned correlation of Weisman (1981) for quenching during reflooding of rod bundles, with the following empirical modifications. In Eq. 81, the constant 0.04 is replaced with 0.02, and the right side of Eq. 83 is multiplied with 0.5. Furthermore, $T_{w,CHF} - T_{sat}$ on the right side of Eq. 81 is replaced with

$$\max\{3K, \min[40K, (T_{w,CHF} - T_{sat})]\} \quad (84)$$

It should be mentioned that in practice during flow transition boiling, the wall heat flux depends on a number of parameters that are not included in the above correlations, including the flow history (i.e., the upstream flow field details, e.g., the distance from the quench front in bottom quenching of hot vertical surfaces), and on the type of the heat transfer process (quasi-steady or transient).

3.3 Stable Film Boiling and Dispersed Flow Film Boiling

Stable Film Boiling. Stable film boiling occurs primarily in the inverted annular flow regime, when a liquid-dominated bulk flow exists. The film boiling process in this case should closely resemble the film boiling process in pool boiling. Stable film boiling can thus be assumed when

$$T_w > T_{\text{MFB}} \quad (85)$$

$$\alpha \leq 0.4, \quad (86)$$

where α is the local void fraction. When stable boiling is encountered, pool film boiling methods are recommended.

Dispersed Flow Film Boiling. Dispersed flow film boiling occurs when the two-phase flow pattern is primarily dispersed droplet. Thermodynamic non-equilibrium (saturated droplets entrained in superheated vapor) is possible. Several mechanisms simultaneously contribute to heat transfer, including convection from wall to vapor, convection and radiation from wall to droplets, convection from vapor to droplets, evaporation from droplets, and droplet impingement on the wall. An accurate and widely used correlation for this regime is (Groeneveld 1973)

$$\frac{hD_H}{k_g} = a \left\{ \text{Re}_g \left[x_{\text{eq}} + \frac{\rho_g}{\rho_f} (1 - x_{\text{eq}}) \right] \right\}^b \text{Pr}_{v,w}^c Y^d \quad (87)$$

$$Y = 1 - 0.1 \left(\frac{\rho_f}{\rho_g} - 1 \right)^{0.4} (1 - x_{\text{eq}})^{0.4} \quad (88)$$

where $\text{Re}_g = GD_H/\mu_g$, $\text{Pr}_{v,w}$ is the vapor Prandtl number at wall temperature, and the heat flux is related to the wall temperature according to

$$q_w'' = h(T_w - T_{\text{sat}}) \quad (90)$$

The constants a , b , c , and d , as well as the range of validity of the correlation, are summarized in Table 1.

Table Look-Up Method for Steam–Water Flow Boiling. For flow boiling of water in vertical tubes, a direct table look-up has been proposed as an alternative to the application of correlations. The tables of Groeneveld et al. (2003) are based on more than 77,000 data points and cover the inverted annular (i.e., stable film boiling) and dispersed flow boiling regimes. The experimental database for these tables covers the following parameter ranges:

$$2.5 \leq D \leq 24.7 \text{ mm}, 12 \leq G \leq 6,995 \text{ kg/m}^2 \cdot \text{s}, \\ -0.1 \leq x_{\text{eq}} \leq 2.0, 0.1 \text{ MPa} \leq P \leq 20 \text{ MPa}.$$

Table 1 Numerical values of the constants in Groeneveld's (1973) correlation

Correlation	a	b	c	d	Pressure (MPa)	Mass flux (kg/m ² ·s)	Quality
Groeneveld 5.7	5.2×10^{-2}	0.688	1.26	-1.06	3.44–10.1	0.8–4.1	0.10–0.90
Goreneveld 5.9	3.27×10^{-3}	0.901	1.32	-1.50	3.44–21.8	0.70–5.30	0.10–0.90

The conditions with $x_{\text{eq}} > 1$ imply thermodynamic nonequilibrium, namely, saturated droplets entrained in superheated vapor. The look-up table of Groeneveld et al. (2003) is available at the Internet site of TCI Thermalhydraulics Consultants Inc. (2017). The heat transfer coefficient should be found from

$$h = h_{D_{\text{ref}}} [P, G, x_{\text{eq}}, (T_w - T_{\text{sat}})] (D_{\text{ref}}/D)^{0.2}, \quad (89)$$

where $D_{\text{ref}} = 8$ mm and $h_{D_{\text{ref}}} [P, G, x_{\text{eq}}, (T_w - T_{\text{sat}})]$ is read from the tables.

4 Cross-References

- ▶ [Boiling and Two-Phase Flow in Narrow Channels](#)
- ▶ [Flow Boiling in Tubes](#)
- ▶ [Nucleate Pool Boiling](#)

References

- Adamson AW, Ling L (1964) The status of contact angle as a thermodynamic property. *Adv Chem Ser* 43:57–73
- Auracher H, Buchholtz M (2005) Experiments on the fundamental mechanisms of boiling heat transfer. *J Braz Soc of Mech Sci Eng* 27(1):1–22. Available on Internet at: <http://www.scielo.br/pdf/jbsmse/v27n1/25372> (July, 2017)
- Auracher H, Marquardt W (2002) Experimental studies of boiling mechanisms in all boiling regimes under steady-state and transient conditions. *Int J Therm Sci* 41:586–598
- Bailey NA (1971) Film boiling on submerged vertical cylinders. AEEW-M1051
- Baumeister KJ, Hamill TD (1967) Laminar flow analysis of film boiling from a horizontal wire. NASA TN D-4035
- Baumeister KJ, Simon FF (1973) Leidenfrost temperature – its correlation for liquid metals, cryogenics, hydrocarbons, and water. *J Heat Transf* 95:166–173
- Berenson PJ (1960) Transition boiling from a horizontal surface. MIT Heat Transfer Lab. Tech. Rpt. No. 17, March 1960
- Berenson PL (1961) Film-boiling heat transfer from a horizontal surface. *J Heat Transf* 83:351–358
- Berenson PJ (1962) Experiments on pool boiling heat transfer. *Int J Heat Mass Transfer* 5:985–999
- Bernardin JD, Mudawar I (1999) The Leidenfrost point: experimental study and assessment of existing models. *J Heat Transf* 121:894–903
- Biance A-L, Clanet C, Quere D (2003) Leidenfrost Drops *Phys Fluids* 15:1632–1637
- Bjonard TA, Griffith P (1977) PWR blowdown heat transfer. In: Jones OC, Bankoff SG (eds) Symposium on thermal and hydraulic aspects of nuclear reactor safety, vol 1. ASME, New York
- Blum J, Marquardt W, Auracher H (1996) Stability of boiling systems. *Int J Heat Mass Transf* 39:3021–3033
- Breen BP, Westwater JW (1962) Effect of diameter of horizontal tubes on film boiling heat transfer. *Chem Eng Prog* 58(7):67–72
- Bromley LA (1950) Heat transfer in stable film boiling. *Chem Eng Prog Symp Ser* 46:221–227
- Bromley LA, LeRoy NR, Robbers JA (1953) Heat transfer in forced convection film boiling. *Ind Eng Chem* 45:2639–2646

- Bui TD (1984) Film and transition boiling heat transfer on vertical surfaces. PhD thesis, University of California at Los Angeles
- Bui TD, Dhir VK (1985a) Transition boiling heat transfer on a vertical surface. *J Heat Transf* 107:756–763
- Bui TD, Dhir VK (1985b) Film boiling heat transfer on an isothermal vertical surface. *J Heat Transf* 107:764–771
- Carey VP (2008) *Liquid–vapor phase-change phenomena*, 2nd edn. CRC Press, New York
- Cassie ABD, Baxter S (1944) Wettability of porous surfaces. *Trans Faraday Soc* 40:546–550
- Chang Y-P (1959) Wave theory of heat transfer in film boiling. *J Heat Transf* 81:1–12
- Chen JC (1966) Correlation for boiling heat transfer to saturated fluids in convective flow. *Ind Eng Chem Res* 5:322–329
- Collier JG (1981) Forced convection boiling. In: Bergles AE, Collier JG, Delhaye JM, Hewitt GF, Mayinger F (eds) *Two-phase flow and heat transfer in power and process industries*. Hemisphere, Washington, DC
- Collier JG, Thome JR (2004) *Convective boiling and condensation*, 3rd edn. Clarendon Press, Oxford
- Dhir VK (1991) Nucleate and transition boiling heat transfer under pool and external flow conditions. *Int J Heat Fluid Flow* 12:290–314
- Dhir VK (1998) Boiling heat transfer. *Annual Rev Fluid Mech* 30:265–401
- Dhir VK, Liaw SP (1989) Framework for a unified model for nucleate and transition pool boiling. *J Heat Transf* 111:739–746
- Dhir VK, Purohit GP (1978) Subcooled film-boiling heat transfer from spheres. *Nucl Eng Des* 47:49–66
- Drew TB, Mueller C (1937) Boiling *Trans AIChE* 33:449–473
- Faghri M, Zhang Y (2006) *Transport phenomena in multiphase systems*. Elsevier/Academic Press, New York
- Fan L-W, Li J-Q, Su Y-Y, Wang H-L, Ji T, Yu Z-T (2016) Subcooled pool film boiling heat transfer from spheres with superhydrophobic surfaces: an experimental study. *J Heat Transf* 138: paper no. 021503
- Farahat MM, Nasr TN (1978) Nature convection film boiling from spheres to saturated liquids, an integral approach. *Int J Heat Mass Transf* 21:256–258
- Forrest E, Williamson E, Buongiorno J, Hu L-W, Rubner M, Cohen R (2010) Augmentation of nucleate boiling heat transfer and critical heat flux using nanoparticle thin-film coatings. *Int J Heat Mass Transf* 53:58–67
- Frederking THK, Clark JA (1963) Natural convection film boiling on a sphere. *Adv Cryog Eng* 8:501–506
- Ghiaasiaan SM (2011) *Convective heat and mass transfer*. Cambridge University Press, Cambridge
- Ghiaasiaan SM (2017) *Two-phase flow, boiling and condensation in conventional and miniature system*. 2nd edn. Cambridge University Press, Cambridge
- Gopalan P, Kandlikar SG (2014) Contact line characteristics of liquid-gas interfaces. *Microfluids Nanofluids* 16:999–1008
- Gottfried BS, Lee CJ, Bell KJ (1966) The Leidenfrost phenomenon: film boiling of liquid droplets on a flat plate. *Int J Heat Mass Transf* 9:1167–1187
- Groeneveld DC (1973) Post-dryout heat transfer at reactor operating conditions. American Nuclear Society Topical Meeting on Water Reactor Safety, Salt Lake City
- Groeneveld DC (1986) The onset of dry sheath condition – a new definition of dryout. *Nucl Eng Des* 92:135–140
- Groeneveld DC, Snoek CW (1986) A comprehensive examination of heat transfer correlations suitable for reactor safety analysis. In: Hewitt GF, Delhaye JM, Zuber N (eds) *Multiphase science and technology*, vol 2. Hemisphere, Washington, DC, pp 181–274
- Groeneveld DC, Stewart JC (1982) The minimum film boiling temperature for water during film boiling collapse. In: *Proceedings of the 7th international heat transfer conference*, vol 4, Munich, 6–10 Sept 1982, pp 303–308

- Groeneveld DC, Leung LKH, Vasic AZ, Guo YJ, Cheng SC (2003) A look-up table for fully-developed film boiling heat transfer. *Nucl Eng Des* 225:83–97
- Hamill TD, Baumeister KJ (1967) Film boiling from a horizontal surface as an optimal boundary value process. In: *Proceedings third international heat transfer conference, Chicago, vol 4*. A.I. Ch.E., New York, pp 59–64
- Haramura Y (1999) Critical heat flux in pool boiling, Chapter 6. In: Kandlikar SG, Shoji M, Dhir VK (eds) *Handbook of phase change*. Taylor and Francis, London
- Hendricks RC, Baumeister KJ (1969) Film boiling from submerged spheres. NASA TND-5124
- Henry RE (1974) A correlation for the minimum film boiling temperature. *AIChE Sympos Ser* 70(138):81–90
- Hohl R, Blum J, Buchholz M, Lüttich T, Auracher H, Marquardt W (2001) Model-based experimental analysis of pool boiling heat transfer with controlled wall temperature transients. *Int J Heat Mass Transf* 44:2225–2238
- Hsu YY, Westwater JW (1960) Approximate theory for film boiling on vertical surfaces. *Eng Prog Symp Ser* 56, 30, 15–24
- Hsu YY, Graham RW (1986) *Transport processes in boiling and two-phase systems*. American Nuclear Society, La Grange Park
- Hwang GS, Kaviany M (2006) Surface wettability change during pool boiling of nanofluids and its effect on critical heat flux. *Int J Heat Mass Transf* 49:844–849
- Johanssen K (1991) Low quality transition and inverted annular flow film boiling of water: an updated review. *Exp Therm Fluid Sci* 4:497–509
- Kalinin EK (1969) Investigation of the crisis of film boiling in channels. In: *Two-phase flow and heat transfer in rod bundles*, ASME Winter annual meeting, Los Angeles, pp 89–94
- Kim JH, Rainey KN, You SM, Pak JY (2002) Mechanism of nucleate boiling heat transfer enhancement from microporous surfaces in saturated FC-72. *J Heat Transf* 124:500–506
- Kim H, DeWitt G, McKrell T, Buongiorno J, Hu L-W (2009) On the quenching of steel and zircaloy spheres in water-based nanofluids with alumina, silica and diamond nanoparticles. *Int J Multiphase Flow* 35:427–438
- Kim H, Buongiorno J, Hu L-W, McKrell T (2010) Nanoparticle deposition effects on the minimum heat flux point and quench front speed during quenching in water-based alumina nanofluids. *Int J Heat Mass Transf* 53:1542–1553
- Klimenko VV (1981) Film boiling on a horizontal plate – new correlation. *Int J Heat Mass Transf* 24:69–79
- Koh JCY (1962) Analysis of film boiling on vertical surface. *J Heat Transf* 84:55–62
- Leonard JE, Sun KH, Anderson JGM, Dix GE, Yuoh T (1978) Calculation of low flow boiling heat transfer for BWR LOCA analysis. Report NEDO-20566–1 Rev. 1. General Electric Company, San Jose
- Liaw SP, Dhir VK (1986) Effect of surface wettability on transition boiling heat transfer from a vertical surface. *Proc Int Heat Transfer Conf, 8th, San Francisco*, 4:2031–2036
- Lienhard JH, Wong PTY (1964) The dominant unstable wavelength and minimum heat flux during film boiling on a horizontal cylinder. *Trans ASME Ser C J Heat Transf* 86:220–226
- Lubin BT (1969) Analytical derivation for total heat transfer coefficient in stable film boiling from vertical plate. *J Heat Transf* 91:452–453
- Moreaux F, Chevrier JC, Beck G (1975) Destabilization of film boiling by means of a thermal resistance. *Int J Multiphase Flow* 2:183–190
- Nagai N, Nishio S (1996) Leidenfrost temperature on an extremely smooth surface. *Exp Therm Fluid Sci* 12:373–379
- Nishio S (1983) Study of minimum heat flux point of boiling heat transfer around a sphere. *Trans Jap Soc Mech Engrs, Ser B* 49:1185–1194
- Nishio S (1987) Prediction technique for minimum-heat flux (MHF) -point condition of saturated pool boiling. *Int J Heat Mass Transf* 30:2045–2057

- Nishio S, Ohtake H (1992) Natural convection film boiling heat transfer (3rd report: film boiling from horizontal cylinder in middle and small diameter regions). *JSME Int J (Series II)* 35:580–588
- Nishio S, Ohtake H (1993) Vapor-film-unit model and heat transfer correlation for natural convection film boiling with wave motion under subcooled conditions. *J Heat Mass Transf* 36:2541–2552
- Nishio S, Uemura M, Sakaguchi K (1987) Film boiling heat transfer and minimum heat-flux (MHF)-point condition in subcooled pool boiling. *JSME Int J Ser B* 30(266):1274–1281
- Nukiyama S (1934) The maximum and minimum values of heat Q transmitted from metal to boiling water under atmospheric pressure. *J Jpn Soc Mech Eng* 37:367–374
- Ohtake H, Koizumi Y (2006) Derivation of correlation and liquid-solid contact model of transition boiling heat transfer. *JSME Int J Ser B* 49(2):343–351
- Olek S, Zvirin Y (1988) The relation between the rewetting temperature and the liquid-solid contact angle. *Int J Heat Mass Transf* 31:898–902
- Patel B, Bell KJ (1966) The Leidenfrost phenomenon for extended liquid masses. *Chem Eng Prog Symp Ser* 62:62–71
- Pron'ko VG, Bulanova LB (1978) Experimental investigation of the thermodynamic crisis of film boiling. *J Eng Phys* 34:534–539
- Ramilison JM, Lienhard JH (1987) Transition boiling heat transfer and the film transition regime. *J Heat Transf* 109:746–752
- Ramu K, Weisman J (1974) A method for the correlation of transition boiling heat transfer data. In: *Proceedings of the fifth international heat transfer conference, Tokyo, vol IV, B4.4*
- RELAP5-3D Code Development Team (2012) RELAP5-3D code manuals, Version 2.3, vols 1–5, INEEL-EXT-98-00834
- Roy Chowdhury SK, Winterton RSH (1985) Surface effects in pool boiling. *Int J Heat Mass Transf* 28:1881–1889
- Sakurai A, Shiotsu M, Hata K (1984). Fastest heat transfer after stable film destruction at the minimum film boiling point. In: *Proceedings of the 21st National Hwt Transfer Svmp, Japan*, pp 469–471
- Sakurai A, Shiotsu M, Hata K (1990a) A general correlation for pool film boiling heat transfer from a horizontal cylinder to subcooled liquid. Part 1 – a theoretical pool film boiling heat transfer model including radiation contribution and its analytical solution. *J Heat Transf* 112:430–441
- Sakurai A, Shiotsu M, Hata K (1990b) A general correlation for pool film boiling heat transfer from a horizontal cylinder to subcooled liquid. Part 2 – experimental data for various liquids and its correlation. *J Heat Transf* 112:442–450
- Segev A, Bankoff G (1980) The role of adsorption in determining the minimum film boiling temperature. *Int J Heat Mass Transf* 23:637–642
- Stewart JC, Groeneveld DC (1981) Low-quality and subcooled film boiling of water at elevated pressures. *Nucl Eng Des* 67:259–272
- TCI Thermalhydraulics Consultants Inc (2017) www.magma.ca/~thermal/
- Tso CP, Low HG, Ng SM (1990) Pool film boiling from sphere to saturated and subcooled liquids of Freon-12 and Freon-22. *Int J Heat Fluid Flow* 11:154–159
- Vakarelski IU, Patankar NA, Marston JO, Chan DYC, Thoroddsen ST (2012) Stabilization of Leidenfrost vapour layer by textured superhydrophobic surfaces. *Nature* 489(7415):274–277
- Vijaykumar R, Dhir VK (1992a) An experimental study of subcooled film boiling on a vertical surface – hydrodynamic aspects. *J Heat Transf* 114:161–168
- Vijaykumar R, Dhir VK (1992b) An experimental study of subcooled film boiling on a vertical surface – thermal aspects. *J Heat Transf* 114:169–178
- Weisman J (1981) Studies of transition boiling heat transfer at pressure from 1–4 bar, EPRI NP-1899

-
- Witte LC, Lienhard JH (1982) On the existence of two transition boiling curves. *Int J Heat Mass Transf* 25:771–779
- Yao S-C, Henry RE (1978) An investigation of the minimum film boiling temperature on horizontal surfaces. *J Heat Transf* 100:260–267
- Zhukov UM, Kazakov GM, Kovalev SA, Kuzma-Kitcha YA (1975) Heat transfer in boiling of liquids on surfaces coated with low thermal conductivity films. *Heat Transf Sov Res* 7(3):16–26
- Zuber N (1959) Hydrodynamic aspects of boiling heat transfer. USAEC Rep AECU-4439